

Heart-on-a-Chip Model of Epicardial–Myocardial Interaction in Ischemia Reperfusion Injury

Dawn Bannerman, Simon Pascual-Gil, Qinghua Wu, Ian Fernandes, Yimu Zhao, Karl T. Wagner, Sargol Okhovatian, Shira Landau, Naimeh Rafatian, David F. Bodenstein, Ying Wang, Trevor R. Nash, Gordana Vunjak-Novakovic, Gordon Keller, Slava Epelman, and Milica Radisic*

Epicardial cells (EPs) form the outer layer of the heart and play an important role in development and disease. Current heart-on-a-chip platforms still do not fully mimic the native cardiac environment due to the absence of relevant cell types, such as EPs. Here, using the Biowire II platform, engineered cardiac tissues with an epicardial outer layer and inner myocardial structure are constructed, and an image analysis approach is developed to track the EPI cell migration in a beating myocardial environment. Functional properties of EPI cardiac tissues improve over two weeks in culture. In conditions mimicking ischemia reperfusion injury (IRI), the EPI cardiac tissues experience less cell death and a lower impact on functional properties. EPI cell coverage is significantly reduced and more diffuse under normoxic conditions compared to the post-IRI conditions. Upon IRI, migration of EPI cells into the cardiac tissue interior is observed, with contributions to alpha smooth muscle actin positive cell population. Altogether, a novel heart-on-a-chip model is designed to incorporate EPs through a formation process that mimics cardiac development, and this work demonstrates that EPI cardiac tissues respond to injury differently than epicardium-free controls, highlighting the importance of including EPs in heart-on-a-chip constructs that aim to accurately mimic the cardiac environment.

1. Introduction

Physiologically relevant models of heart tissue enable the investigation of heart development and disease, as well as testing of potential therapeutic agents. Increasingly complex three-dimensional cardiac tissue constructs developed in microscale platforms, called heart-on-a-chip platforms, are sought after because they can incorporate multiple cell types, directionally dependent chemical, electrical, and mechanical cues, and structural support elements at various scales such that the native tissue is better recapitulated. Heart-on-a-chip platforms can also overcome issues of species variability, relying on the use of human pluripotent stem cell derived progeny, and open the potential for personalized studies, in potentially high throughput configurations.

Bioengineers generating engineered cardiac tissue seek to impart it with key features that are hallmarks of maturity including evidence of organized myocardial sarcomere structures and regular contractile

D. Bannerman, K. T. Wagner, M. Radisic
Chemical Engineering and Applied Chemistry
University of Toronto
Toronto, ON M5S 3E5, Canada
E-mail: m.radisic@utoronto.ca

D. Bannerman, S. Pascual-Gil, Q. Wu, Y. Zhao, S. Okhovatian, S. Landau,
N. Rafatian, D. F. Bodenstein, Y. Wang, M. Radisic
Institute of Biomedical Engineering
University of Toronto
Toronto, ON M5S 3E2, Canada

D. Bannerman, S. Pascual-Gil, Q. Wu, Y. Zhao, K. T. Wagner,
S. Okhovatian, S. Landau, N. Rafatian, D. F. Bodenstein, Y. Wang,
S. Epelman, M. Radisic
Toronto General Health Research Institute
University Health Network
Toronto, ON M5G 2C4, Canada
I. Fernandes, G. Keller
Department of Medical Biophysics
University of Toronto
Toronto, ON M5G 1L7, Canada
I. Fernandes, G. Keller
McEwen Stem Cell Institute
University Health Network
Toronto, ON M5G 1L7, Canada

D. F. Bodenstein
Department of Pharmacology and Toxicology
University of Toronto
Toronto, ON M5G 2C8, Canada
G. Vunjak-Novakovic
Department of Medicine
Columbia University
New York, NY 10032, USA

 The ORCID identification number(s) for the author(s) of this article can be found under <https://doi.org/10.1002/adhm.202302642>

© 2024 The Authors. Advanced Healthcare Materials published by Wiley-VCH GmbH. This is an open access article under the terms of the [Creative Commons Attribution-NonCommercial](https://creativecommons.org/licenses/by-nc/4.0/) License, which permits use, distribution and reproduction in any medium, provided the original work is properly cited and is not used for commercial purposes.

DOI: 10.1002/adhm.202302642

function. Furthermore, while the contraction of cardiac tissue is accomplished by cardiomyocytes (CMs), various other cell types are present in native tissue, contributing to cardiac tissue structure,^[1,2] and engaging in cellular crosstalk.^[3] For example, fibroblasts (FBs) play an important supporting role and affect cardiac function^[4,5] and endothelial cells (ECs) and vascular smooth muscle cells (vSMCs), which form microvessels and vasculature, also contribute to cardiac structure and function.^[6,7]

Although most heart-on-a-chip systems mimic only the myocardium, the epicardium is being recognized as highly important during both development and disease.^[8] The epicardium is the outer layer of the heart, and it is comprised of epithelial cells specific to the heart called epicardial cells (EPIs).^[9] During development, EPIs undergo a process of epithelial-to-mesenchymal transition (EMT) to transform into various cell types including FBs, vSMCs, and a small population of ECs.^[8] These epicardial-derived cells (EPDCs) provide trophic support to CMs during development, with evidence of promoting CM proliferation and maturation.^[10] After development, the epicardium becomes dormant,^[8] but upon injury such as myocardial ischemia, EPIs are activated and begin to re-express fetal gene programs. While the final contribution of re-activated epicardial cells to various cell types after injury is still under debate, migration of the re-activated EPIs occurs as a response to injury.^[9] These re-activated EPIs provide paracrine factors contributing to post-myocardial infarction cardiac remodeling.^[11] For these reasons, heart-on-a-chip systems that include EPIs are needed. Furthermore, the onset of injury is of particular interest to be modeled using these systems since the epicardium plays a crucial role in this process.

Various heart-on-a-chip models have been developed, including the “I-Wire” system,^[12] a centrifugal heart-on-a-chip system,^[13] an extracellular matrix derived engineered heart tissue system,^[14] and the “milliPillar” system.^[15] We have previously developed the Biowire II platform, with non-invasive recording of contractile properties of engineered heart tissues formed in microwells between a pair of anchoring polymer microwires.^[16] Contractile properties of the cylindrical cardiac tissue are evaluated in the system by quantifying the deflection of the polymer wires during tissue contraction and conversion to force values via previously generated force/displacement curves.

Here, we sought to develop a cardiac platform that incorporates the highly relevant EPIs, in a physiologically relevant lo-

calization to facilitate the study of their roles in cardiac tissue formation, injury, and recovery. Currently, heart-on-a-chip models that incorporate EPIs are limited to self-assembled human heart organoids that include epicardial cells,^[17] human induced pluripotent stem cell (hiPSC)-derived premature epicardial cells in co-culture with CMs in 3D spheroids,^[18] and one system of human embryonic stem cell-derived epicardial cells in engineered heart tissue.^[19,20] Establishing a defined localization of the inner myocardial and outer epicardial layer has not been routinely achieved.

The Biowire II system has been shown to be effective for disease modeling of left ventricular hypertrophy^[16,21] and myocardial fibrosis.^[22] Given that myocardial ischemic injury leading to myocardial infarction (MI) is one of the leading causes of death in the developed world,^[23] we sought to model this type of injury in our system. Currently, the most effective clinical treatment approach to improve outcomes after MI is to achieve rapid reperfusion of the occluded artery to restore blood flow to the region. However, this reperfusion stage also causes significant damage—termed ischemia-reperfusion injury (IRI).^[24,25] Establishing effective heart-on-a-chip models of ischemic injury enables investigations of the impacts of MI and IRI on cardiac tissues as well as possible treatment approaches to promote recovery of cardiac function. Previously, Chen et al. developed an acute model of IRI for engineered human EPI-free myocardial tissues and assessed potential strategies for cardioprotection.^[26] We sought to determine whether a similar approach would be applicable in our Biowire II platform with EPI cardiac tissues, with the aim to assess tissue recovery over a prolonged time period and the contribution of a defined epicardial outer layer to functional recovery after IRI in vitro.

Here, we developed a novel model of cardiac tissue that contains both epicardial and myocardial tissue. Cardiac tissues were subsequently assessed under normoxic conditions and conditions mimicking IRI. We found several differences in EPI cardiac tissues compared to the control tissues, including migration of EPIs into the tissue core in a manner that mimics developmental processes, with retention but decreased expression of epicardial marker, and delayed but eventual advancement of functional properties. EPI biowires also experienced less severe injury and as a result less subsequent recovery after IRI. Finally, EPI cell retention and co-localization with myofibroblast markers was increased in injured EPI biowires compared to healthy EPI biowires; altogether, supporting the concept that inclusion of EPIs in such cardiac tissue constructs is important for the study of development and disease.

2. Results

2.1. Epicardial Cell Differentiation

Epicardial cells were generated from human embryonic stem cells (hESC) according to a procedure adapted from a published protocol.^[27] At confluence, cells exhibited some heterogeneity, but the cobblestone morphology typical of epicardial cells was observed (**Figure 1B**). Immunostaining revealed that $70.5 \pm 4.8\%$ of the cells had positively stained nuclei for transcription factor WT1, a marker of epicardium in the context of cardiac tissue, and $92.6 \pm 7.5\%$ of cells possessed ZO-1+ borders, a marker

T. R. Nash
Vagelos College of Physicians and Surgeons
Columbia University
New York, NY 10032, USA

T. R. Nash, G. Vunjak-Novakovic
Department of Biomedical Engineering
Columbia University
New York, NY 10027, USA

S. Epelman
Division of Cardiology
University Health Network
Peter Munk Cardiac Centre
Toronto, ON M5G 2N2, Canada

S. Epelman
Ted Rogers Centre for Heart Research
Toronto, Ontario M5G 1M1, Canada

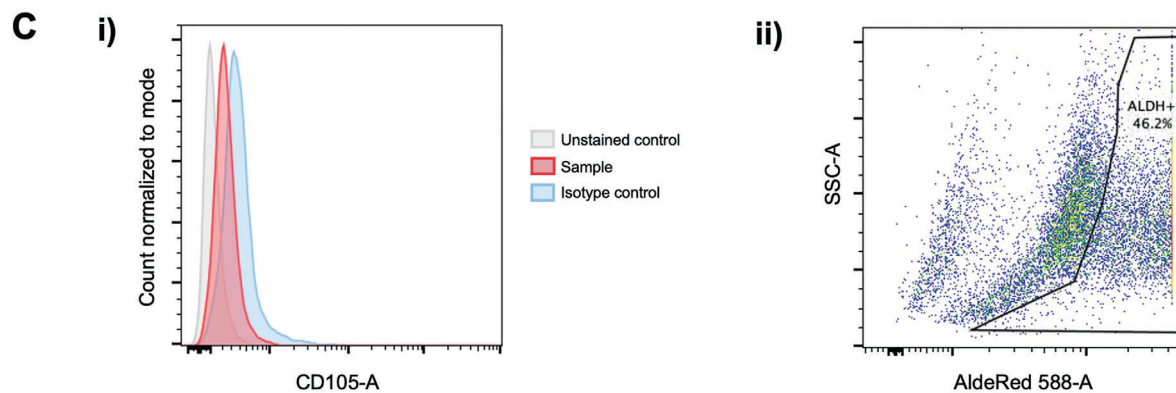
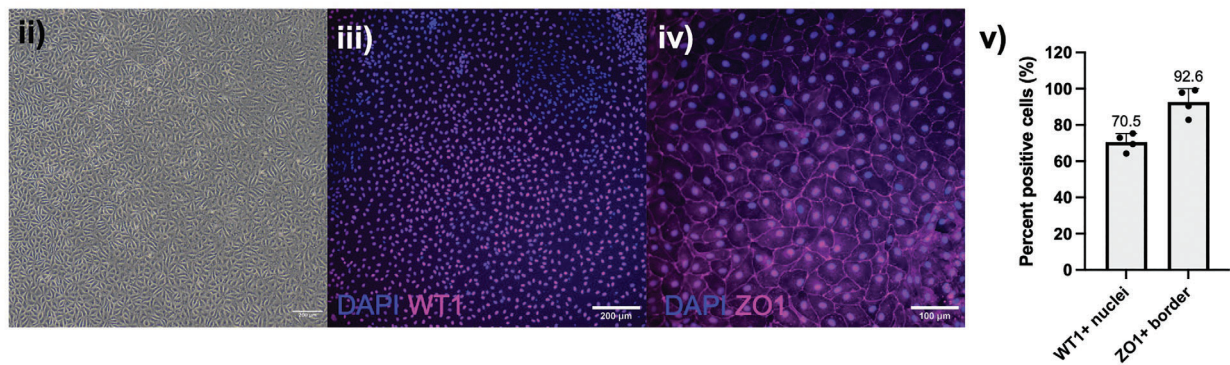
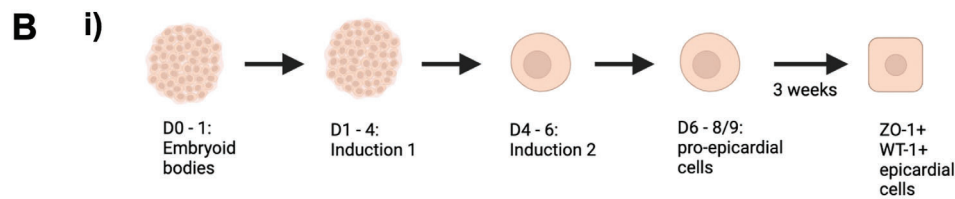
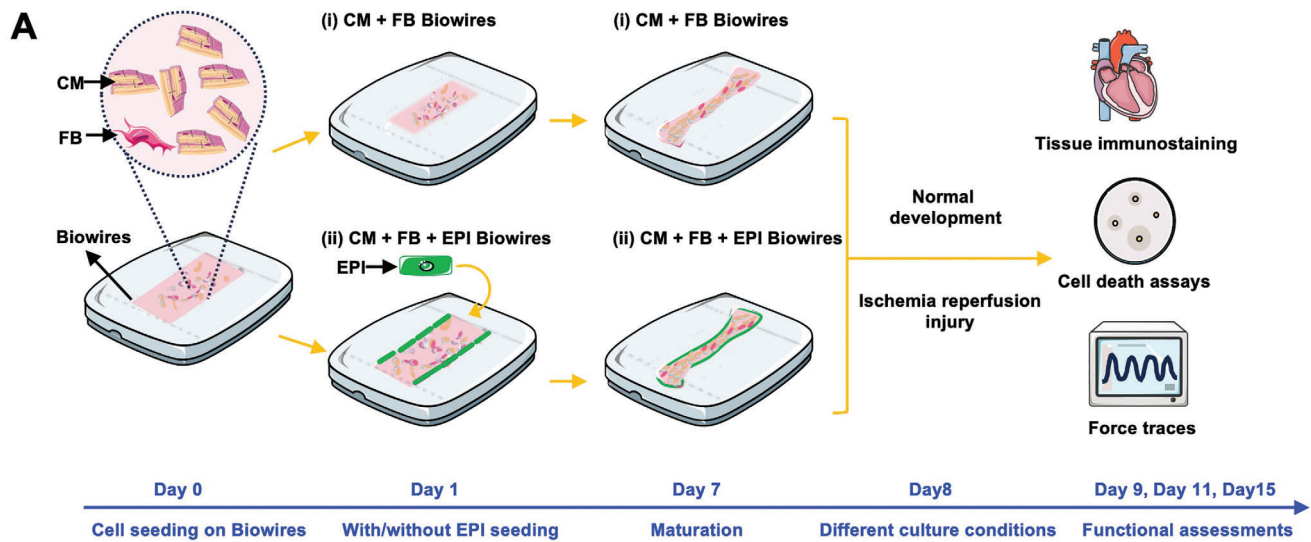


Figure 1. Cardiac tissues were generated with cardiomyocytes, fibroblasts and differentiated epicardial cells, followed by processes of normal development and ischemia reperfusion injury. A) Schematic demonstrating cell composition of biowires and subsequent development and injury modeling. B) Human epicardial cells following i) differentiation protocol (created with Biorender.com) with ii) cells shown as brightfield image, iii) WT1 immunostaining and iv) ZO1 immunostaining. v) Quantification of percent WT1+ nuclei and ZO1+ bordered cells is included ($n = 4$). C) Flow cytometry analysis of i) CD105 and ii) AldeRed (ALDH) expression in the epicardial cells after differentiation.

of tight junctions in epithelial cell sheets (Figure 1B). Flow cytometry analysis demonstrated the cells were negative for mesenchymal marker, CD105, and a significant proportion (46.2%) stained positive for AldeRed, a marker of aldehyde dehydrogenase (ALDH) activity that is used to identify EPI cells^[27] (Figure 1C). This is consistent with values reported for hESC-derived EPIs, ranging from over 40%^[28] to 78.9%,^[27] and in contrast to the cells undergoing EMT, which in the same work were reported to range from 1.4% to 35% ALDH+.^[27] Some heterogeneity is common in the differentiation of stem cells to the epicardial lineage, and presence of small populations of EPDC may exist. For simplicity in this paper, we will subsequently refer to the hESC-derived cells produced from this method and used in the subsequent experiments as epicardial cells (EPIs), despite their maturity and phenotype shifting throughout the following stages due to the co-culture in cardiac constructs and varying treatments.

2.2. Epicardial Biowire Formation

The EPIs generated using the recently established methods (Figure 1B) were incorporated into biowire cardiac tissues using a two-step seeding protocol in order to mimic the spatial arrangement of epicardium surrounding the myocardium (Figure 1A and Figure 2A). Key cells included in the biowire constructs, CMs and EPIs, were derived from human pluripotent stem cells, and the number of contracting cells (i.e., CMs) was kept consistent between the EPI biowire and control biowire groups. One day after seeding CMs and FBs, some tissue compaction was observed with tissue width reduced to $75 \pm 12\%$ of well width (Figure 2A). EPIs were then seeded around the tissues to form EPI biowires (CM+FB+EPI group), while control biowires did not have EPIs added (CM+FB group). EPIs surrounded the tissue and at early time points (e.g., day 2), there was a clear distinction between the EPIs and the CM+FB tissue within the biowires (Figure 2B). EPIs provided a level of support for forming biowires, demonstrated by the number of tissues remaining attached to the microwires (which were present on both sides of the microwells for tissue attachment) being significantly greater in the CM+FB+EPI group than in the CM+FB group at day 8. While the CM+FB tissues had lower attachment rate ($39.8 \pm 10.8\%$) compared to our previous reports,^[29] differences in CM cell line, CM to FB ratio, and electrical conditioning procedures are possible reasons for this. Nevertheless, for the group that had a similar ratio of myocytes to non-myocytes compared to our previous report (i.e., the CM+FB+EPI tissues), similar attachment rates were observed as in our previous reports, with $74.6 \pm 4.5\%$ of CM+FB+EPI tissues remaining attached (Figure 2C). The differences in cell number and composition, with EPI biowires having higher cell numbers than control biowires is another likely reason for the differences between groups. Over the next week, tissues continued to compact and tissue width decreased over time within both groups (Figure 2D). Although EPI cardiac tissues had slightly greater diameter than the control tissues at earlier time points, which can be explained by the presence of additional cells in coculture, both groups leveled off after several days and no difference in tissue diameter was observed after one week, the time period when

initial tissue remodeling due to cell/gel compaction is generally complete.

The GFP+ EPIs could be visualized surrounding the EPI biowires initially (Figure 2E-i). Interestingly, EPIs were observed to be moving into the center of the biowires over time (Figure 2E, and Figures S2 and S3, Supporting Information). During the first week of tissue formation following EPI introduction, profiles of the average GFP+ pixel distribution through the width of the cardiac tissue show the transition of these cells from the outside edges at earlier time points toward the center at later time points (Figure 2E-iii, Figures S3 and S4, Supporting Information). By quantifying the slopes of these profiles, we observed a significant increase over time, confirming the movement of EPI cells from the exterior (i.e., negative slope) to the interior (i.e., positive slope) of the tissues (Figure 2E-iv).

One week after the EPI cell seeding on day 8, the tissues were assessed for functional properties. Active tension, active to passive tension ratio (which considers factors associated with passive tension such as tissue stiffness), and contraction slope were compared between the control tissues and EPI cardiac tissues (Figure 2F-i-iii; passive tension shown independently in Figure S5B, Supporting Information). A significantly lower active to passive tension ratio was observed in the EPI biowire group. Other contractile properties were comparable between the two groups although there was a trend of lower properties in the EPI biowire group. However, excitation threshold (ET), representing the minimum excitation voltage for synchronous beating, and maximum capture rate (MCR), the maximum frequency that tissues can beat synchronously, were not significantly different between the control tissues and EPI cardiac tissues (Figure 2F-iv,v).

2.3. Characterization of Epicardial Biowires under Baseline Conditions

Following the initial assessments of functional tissue properties at day 8, further measurements were assessed relative to day 8 data to capture the evolution of the tissues over longer periods of time. Under baseline culture conditions, tissue diameter remained relatively stable in the EPI biowire group, with more compaction occurring in control tissues despite having fewer non-myocytes (Figure 3A,B). With time in culture, active tension increased in both groups as expected due to tissue maturation (Figure 3C,D). The active to passive tension ratio and contraction slope only increased over time in the EPI biowire group. Comparisons between control tissues and EPI cardiac tissues at each time point (indicated by # in Figure 3B,D and shown in Figure S6, Supporting Information) revealed that the EPI biowires did not exhibit significant differences in any of properties by day 15, including in the active to passive tension ratio, for which the EPI biowire group caught up to match the control biowire group over time. Both groups exhibited a significant decrease in MCR with time in culture (Figure S7, Supporting Information), as expected due to the lack of electromechanical conditioning. A slight but significant increase in ET was observed in EPI biowires at day 15 compared to day 8 (Figure S7, Supporting Information), which may be explained by the lack of electrical conditioning—a variable that was not in the scope of this study.^[29]

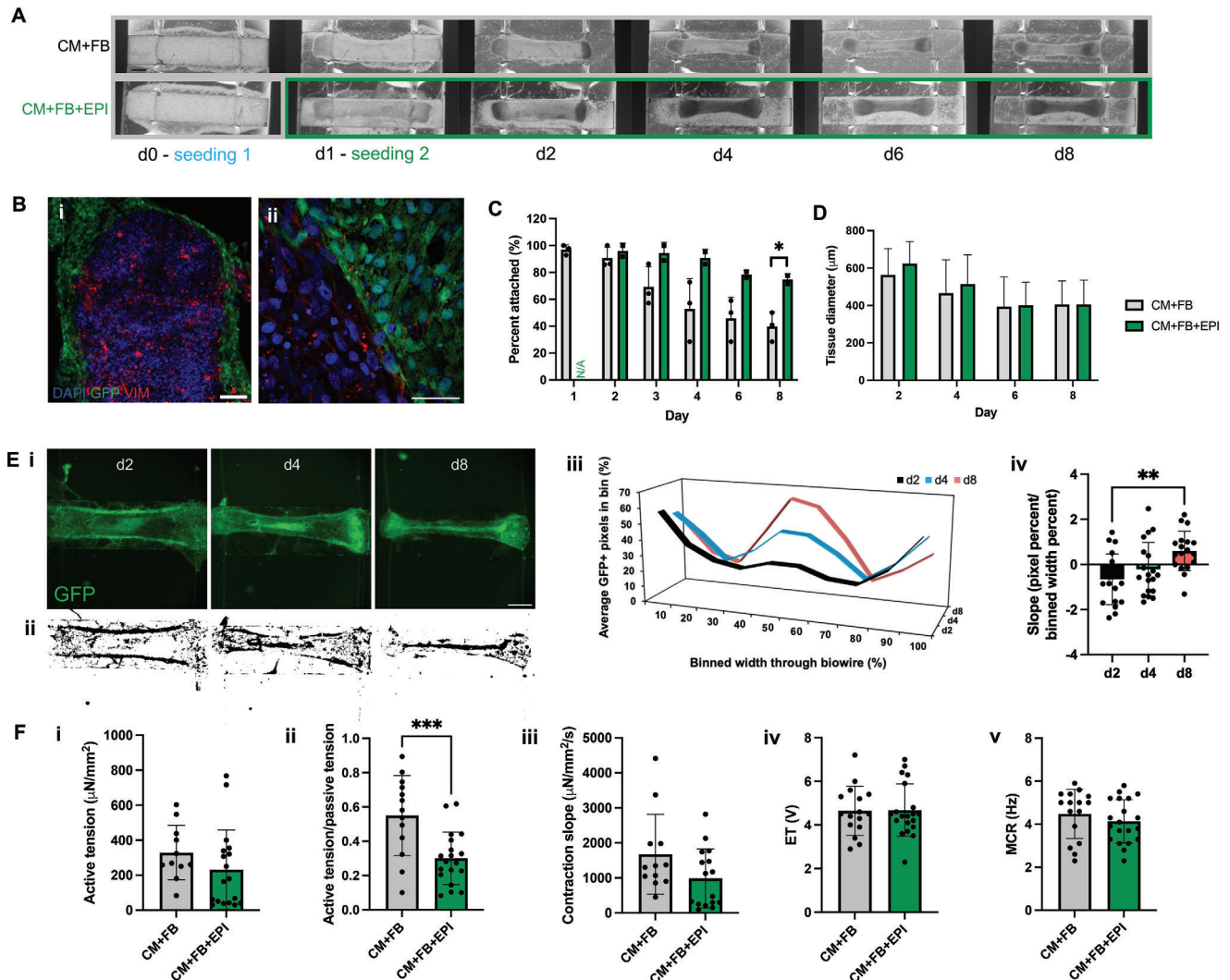


Figure 2. Engineering of cardiac tissues with defined epicardial/myocardial layers and tracking of EPI cell migration over 8 days. A) Representative images of cardiac tissues illustrating the double seeding procedure and tissue compaction. Scale bar is 500 μm. B) Vimentin stained biowires at day 2 (i.e., one day after EPI seeding) showing i) the end of a tissue and ii) a region with clear EPI and CM+FB sections. Scale bars are 100 μm (i) and 50 μm (ii). C) Percentage of tissues remaining attached to the microwires in microwells. Average values from three batches of CM+FB biowires and 2 batches of CM+FB+EPI biowires are shown with unpaired *t* tests between groups at each time point. N per batch are CM+FB: 14, 7, 22; CM+FB+EPI: 36 and 21. D) Tissue diameter of control CM+FB cardiac tissues ($n = 18$ at day 2, $n = 15$ by day 8) and CM+FB+EPI cardiac tissue ($n = 20$) over time. A mixed-effects model (REML) with Šidák's multiple comparison test was performed. E) GFP+ epicardial cells imaged in the green channel surrounding in the composite tissues on i) day 2, 4, and 8 with ii) corresponding thresholded image for GFP+ pixel tracking. Scale bar is 500 μm. iii) Profiles of the average GFP+ pixels in the binned width through the tissue are shown and iv) the slopes of the positive pixels profiles over the first 50% binned width were compared. An ordinary one-way ANOVA with Tukey's multiple comparisons test was performed ($n = 19$ or 18). F) Functional properties of tissues on day 8 are compared. i) Active tension with Mann-Whitney test (CM+FB $n = 11$ and CM+FB+EPI $n = 18$), ii) active tension per passive tension with unpaired *t* test (CM+FB $n = 13$ and CM+FB+EPI $n = 19$), iii) contraction slopes with Mann-Whitney test (CM+FB $n = 12$ and CM+FB+EPI $n = 16$), iv) ET with unpaired *t* test (CM+FB $n = 16$ and CM+FB+EPI $n = 20$), and v) MCR with unpaired *t* test (CM+FB $n = 16$ and CM+FB+EPI $n = 20$) are shown.

There was no significant difference observed in the myocardial architecture between the groups with and without EPIs. Both groups displayed aligned sarcomere structures, with no measured differences in cardiac troponin T (cTnT) density or eccentricity (Figure 3E). The presence of GFP+ EPI cells was shown throughout the myocardial parenchymal tissue. Spindle-shaped morphology was observed in GFP+ cells dispersed throughout the tissue.

To understand the response of EPIs after their addition into biowires, expression of epicardial marker, WT1, was assessed in the tissues and compared over time. WT1 is used to discern developing epicardium from other developing cardiac layers, and its expression can indicate retention of the epicardial phenotype, while its downregulation can indicate subsequent progression through EMT.^[18,19,27,28] Immunostaining of CM+FB+EPI biowires at day 2 reveal GFP+ cells concentrated around the

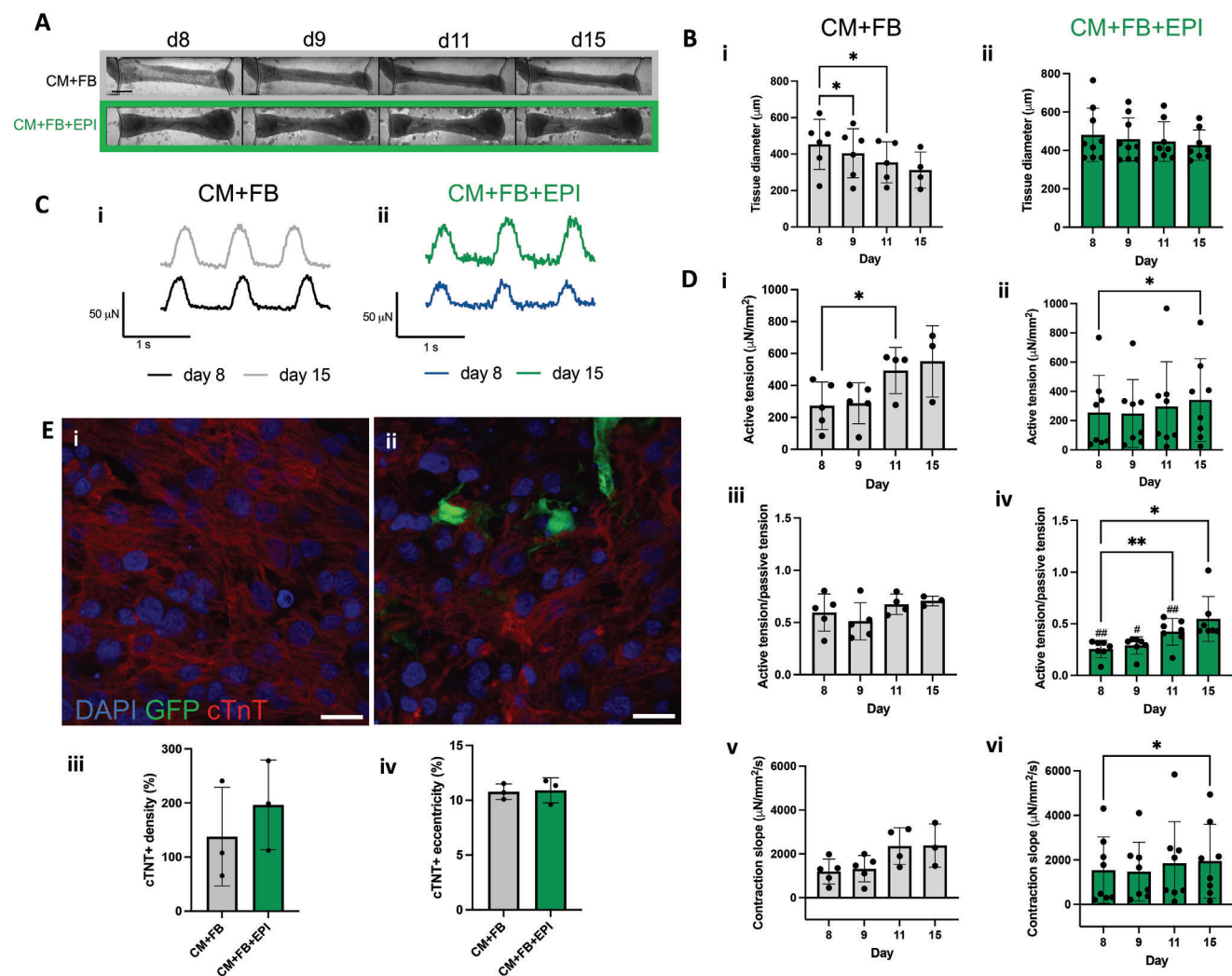


Figure 3. Epicardial and control cardiac tissues exhibit similar functional properties over time under baseline normoxic conditions. A) Images of cardiac tissues over time. Scale bar is 500 μm . B) Tissue diameter over time in the i) control CM+FB cardiac tissues and ii) CM+FB+EPI cardiac tissues with mixed-effects analysis using REML and Dunnett's multiple comparisons test ($n = 6$ for CM+FB and $n = 9$ for CM+FB+EPI at d8). C) Force traces of CM+FB control i) cardiac tissues and ii) CM+FB+EPI cardiac tissues at day 8 and 15. D) Functional properties of cardiac tissues over time. Active tension, active tension over passive tension, and contraction slope are shown for CM+FB control tissues (i**, iii**, and v**, respectively) and CM+FB+EPI tissues (ii*, iv*, and vi*, respectively). *Repeated measures one-way ANOVA with Dunnett's multiple comparisons tests was applied comparing to the initial time point. **When values were missing, data were analyzed with a mixed-effects model (REML) with Dunnett's multiple comparisons test. # indicates statistical significance in pairwise comparisons from CM+FB control group at the same time point. E) Immunofluorescence images of i) CM+FB control and ii) CM+FB+EPI cardiac tissues at endpoint, showing presence of cTnT staining and GFP+ epicardial cells. Nuclei were counterstained with DAPI. Scale bar is 20 μm . Quantification of cTnT iii) density and iv) eccentricity are shown, with unpaired t test applied.

border of the biowire, as well as a strong presence of WT1+ nuclei in the same regions (Figure 4A). The CM+FB+EPI tissues after two weeks in culture show GFP+ cells more distributed through the tissue, and retained WT1+ nuclei within the GFP+ region. Analysis of higher magnification regions confirm these trends (Figure 4B) and indicate that the overall percent of WT1+ cells in the tissues is significantly lower at endpoint compared to at day 2 (Figure 4C-i), even more significantly than total cell count (Figure 4C-ii). However, when WT1+ cells are compared relative to the number of GFP+ cells, the WT1+ presence in endpoint biowires is only slightly, and insignificantly lower (Figure 4C-iii). Nevertheless, the intensity of the WT1 signal decreases in the tissues over time (Figure 4C-iv). Taken together, these results sug-

gest that while there is retention of epicardial marker WT1 over time in the tissues, downregulation likely occurs to some extent.

2.4. Ischemia-Reperfusion Injury of Biowires

IRI was simulated in the tissues on day 8 by performing a 6-h period of ischemic culture in hypoxia (i.e., 95% N_2 , 5% CO_2) and nutrient deprivation media, followed by a 3-h period of culture in normoxia (i.e., 5% CO_2) and reperfusion media, based on previous work validating this model for tissue-engineered constructs.^[26] Visual observations immediately following ischemia indicated that injured tissues were not beating. Beating

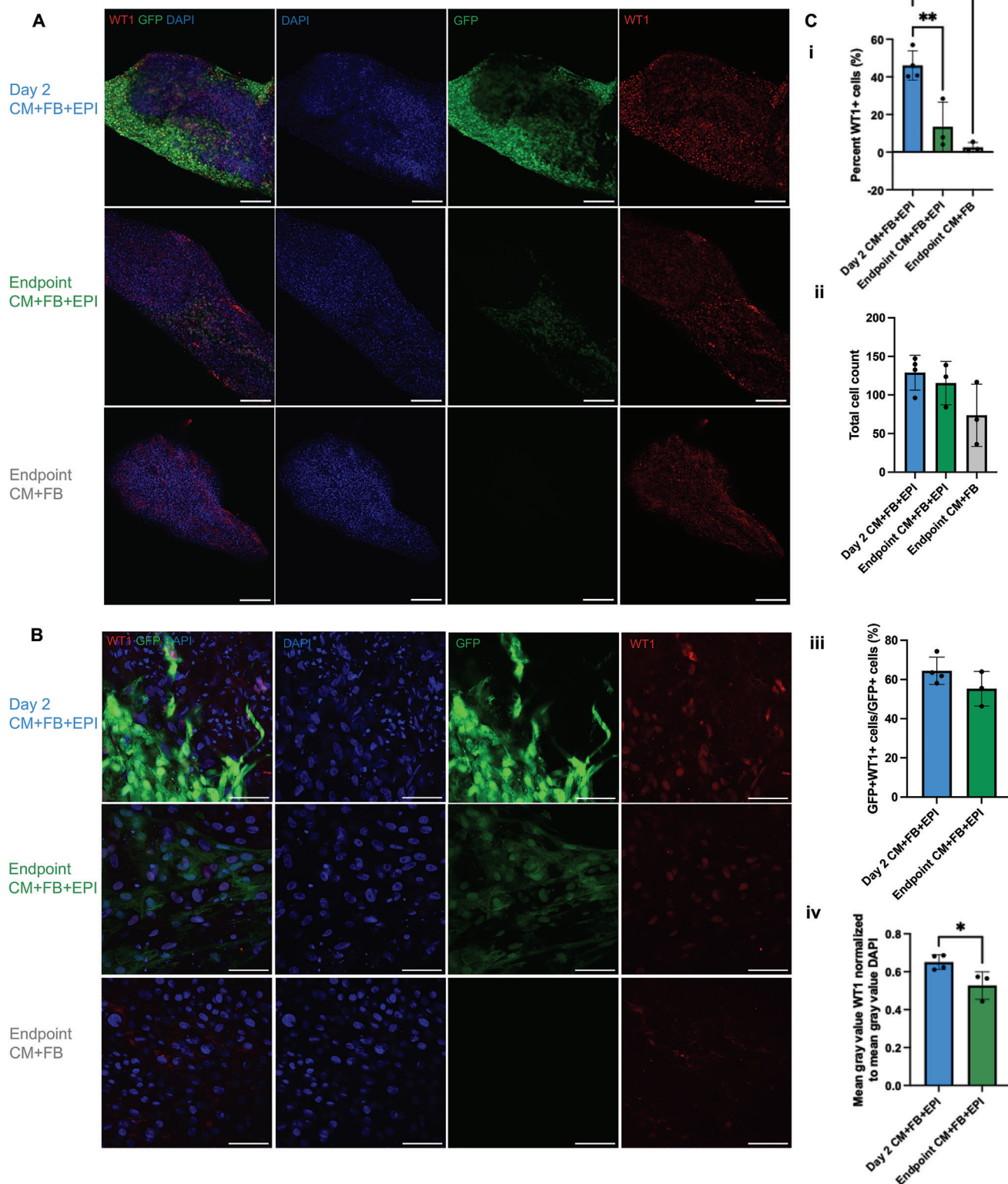


Figure 4. Epicardial marker WT1 presence is retained but reduced in biowires over time. A) Representative confocal images of WT1 stained (red) biowire tissues. Scale bar is 200 μm . B) Representative confocal images of WT1 stained (red) regions within the biowire tissues. Scale bar is 50 μm . C) Quantification of immunofluorescence images showing i) WT1+ cell percent of total (*), ii) total cell count (*), iii) WT1+ cell percent of GFP+ cells (**), and iv) mean gray value of the WT1 channel relative to the mean gray value of the DAPI channel (**). Ordinary one-way ANOVA with Tukey's multiple comparisons test (*) or unpaired t test (**) were performed. EPI cells are visualized by GFP signal. Nuclei were counterstained with DAPI.

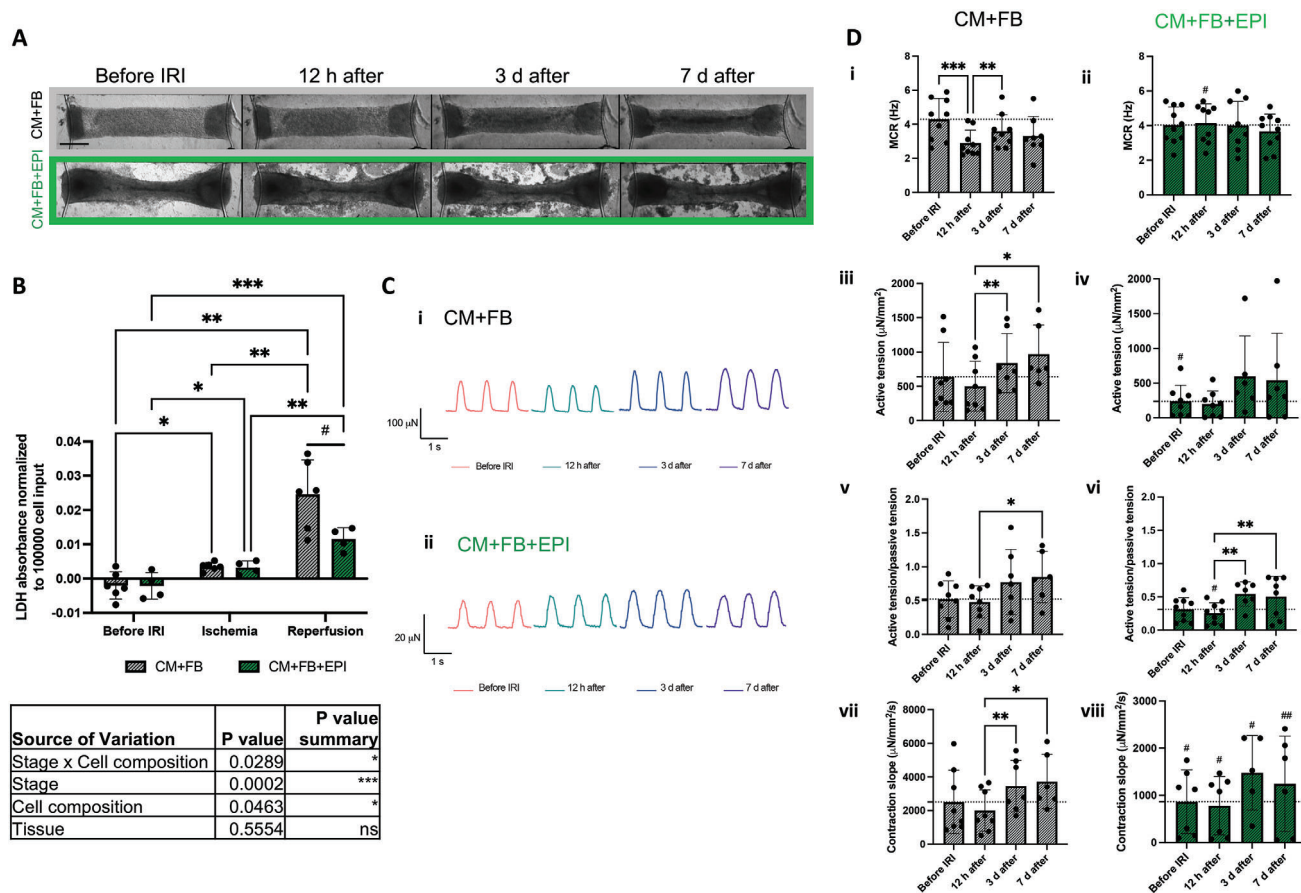


Figure 5. Epicardial cardiac tissues experience fewer changes after IRI compared to control cardiac tissues and as a result exhibit less significant recovery of functional properties over time. A) Images of cardiac tissues before IRI, 12 h after, 3 d after, and 7 d after IRI. Scale bar is 500 μm . B) LDH released from cells in culture media during three stages: 24 h before IRI, during ischemia, and during reperfusion, normalized to 10^5 cell input during tissue formation. Two-way ANOVA with Tukey's multiple comparison test was applied, and results are shown on the graph and in the table. # indicates significant differences of unpaired t-test between groups at each time point. C) Force traces of representative samples in i) CM+FB cardiac tissues and ii) CM+FB+EPI cardiac tissues before IRI and at three time points afterward. D) Electrical excitability and functional properties of cardiac tissues over time. MCR, active tension, active tension over passive tension, and contraction slope are shown for CM+FB biowires (i, iii, v, vii, respectively) and CM+FB+EPI biowires (ii, iv, vi, viii, respectively). Mixed-effects model (REML) with Dunnett's multiple comparisons test was applied comparing to the 12 h after IRI values. Dotted lines correspond to the average of the properties before IRI. # indicates statistical significance in pairwise comparisons from CM+FB control group at the identical time point.

recovered after the reperfusion period. Cell death during these periods was confirmed by comparing LDH absorbance during a 24-h period before IRI, during ischemia, and during reperfusion (Figure 5B). In line with previous reports of establishing IRI in human engineered tissue constructs,^[26] as well as established in vivo understanding of IRI,^[24,25] the period of greatest cell death was during reperfusion, with some cell death also occurring during ischemia, and negligible cell death in the 24-h period before IRI. Interestingly, the EPI cardiac tissues had significantly less cell death during reperfusion compared to the control tissues, as evidenced by LDH measurements (Figure 5B).

Functional properties were also compared before and after IRI and directionally lower average electrical and force properties were observed in all groups in nearly all assessments at the 12-h point after injury compared to before IRI, as demonstrated in the representative force traces (Figure 5C) and functional properties with values below the dotted line representing the baseline values before injury (Figure 5D, and Figure S8, Supporting

Information). Of note, MCR 12 h after IRI compared to before IRI was significantly lower in the control biowire group, whereas no difference was observed in the EPI biowire group. Comparing between the groups at 12 h, EPI cardiac tissues had a significantly higher MCR than control biowires (indicated by # in Figure 5D and in Figure S9, Supporting Information). A higher MCR within a physiological range is considered a good functional outcome, as it indicates that tissues contract simultaneously at high frequency—a property of mature and well-functioning cardiac tissue. The significant decrease in MCR after injury in the CM+FB group indicates worsening performance of the tissue in terms of MCR as a metric. However, the lack of decrease in MCR observed after injury in the CM+FB+EPI group suggests that EPI cells may protect the tissues ability to contract in unison at higher frequencies.

The effects of the IRI regimen on EPI biowires were also explored using another source of CMs, BJ1D-iPSC derived CMs, to establish more general applicability of the injury model that

moves beyond one cell line. In this case, more dramatic effects were observed, likely a result of the use of a cell line more sensitive to injury, and consistent with cell line variability that is often observed with human pluripotent stem cells (Figure S10, Supporting Information). In tissues formed with BJ1D-iPSC derived CMs, FBs, and EPIs, deterioration of electrical and functional properties was observed 12 h after IRI. At three days after IRI, half of the tissues were no longer beating, representing an even more severe injury outcome.

Differences in the response to IRI over time were observed in the EPI cardiac tissues compared to the control tissues. Recovery can be seen in many of the electrical and contractile properties over time for both biowire groups, with visible improvements at 3 and 7 days after IRI compared to the at 12-h after IRI time point (Figure 5C,D). The recovery of the functional properties of active tension and contraction slope that occurs by 7 days after IRI relative to before IRI was not significant in the EPI biowire group, whereas the control biowires demonstrate significant recovery over time (Figure 5D).

2.5. Epicardial Cell Tracking in Healthy and Injured Epicardial Biowires

Focusing on the EPI cardiac tissues before and after IRI and comparing them to the time-matched EPI cardiac tissues that did not undergo IRI (termed No IRI control), we tracked GFP+ cells within biowires (Figure 6A). Under normal conditions (i.e., No IRI), overall coverage of GFP+ cells at day 15 was significantly lower than the coverage at day 8 (Figure 6B-i). Moreover, the internal peak of the GFP+ profiles within the tissues plateaued in the No IRI controls, indicating no increase in cell migration (Figure 6C and Figure S11A, Supporting Information). Indeed, the average internal GFP+ profile slope decreased over time in the No IRI controls (Figure 6B-iii, and Figure S11B, Supporting Information). In contrast, the tissues that underwent IRI continued to display more coverage of GFP+ cells at day 15 compared to day 8 (Figure 6B-ii) along with a stronger presence of a GFP+ cell core with steeper internal cell concentration profiles, which remained stable over time (Figure 6B-iv,C and Figure S11A,B, Supporting Information). No significant differences were observed for GFP+ cell coverage specifically at the edge of the tissues (Figure S11C,D, Supporting Information). Analysis of GFP+ distribution in biowire tissues demonstrate similar trends in terms of appearance, GFP+ density, and GFP+ cell cluster distance from the longitudinal center of the tissue (Figure 6E,D). Thus, it appears that EPIs in the biowire cores diminished over time in the No IRI control EPI tissues but remained present in the EPI biowires undergoing IRI.

Probing deeper into the expression of EMT-associated markers, alpha smooth muscle actin (α -SMA) and vimentin, some differences between IRI-treated EPI tissues and No IRI control EPI tissues were observed (Figure 7). Both endpoint groups had significantly lower GFP+ density compared to the earlier time-point biowires (Figure 7A,C-i,E-i). In both endpoint groups, the GFP-expressing cells possessed morphologies consistent with the mesenchymal phenotype (Figure 7B,D). No significant differences were detected in α -SMA expression between the early time-point, No IRI endpoint control, and IRI endpoint groups

(Figure 7C-ii), suggesting that the total amount of α -SMA does not significantly change over time. However, notably, a significant difference in the fraction of α -SMA cells that colocalize with GFP expression was observed in the group that underwent IRI (Figure 7C-iii), suggesting EPI cell contribution to myofibroblasts, which orchestrate repair after injury such as an MI, but could also promote fibrosis in cases of overactivation. The trend of increased α -SMA+ eccentricity, indicating organized α -SMA presence, in the endpoint IRI group further corroborates this result (Figure 7C-iv). There are no notable differences in vimentin colocalization with GFP+ signal or eccentricity between groups (Figure 7E-iii,iv), but the total vimentin density is highest in the day 2 tissues (Figure 7E-ii), which we hypothesize is a result of the FBs initially present in the tissues expressing vimentin, and subsequently becoming more dilute within a tissue over time when integration of EPI cells and CM+FB cells occurs, in contrast to the distinct EPI and CM+FB regions that exist at early time points (Figure 7A).

3. Discussion

The recent discovery of differentiation pathways to derive EPIs from human induced pluripotent and embryonic stem cells,^[18,19,27] has enabled the use of this cell type in miniature 3D tissue constructs, thus capturing the complex, multilayer native cardiac structure more closely. The novelty of this work lies in the generation of a multi-layer cardiac tissue model with an initial outer epicardial compartment that migrates inward in the tissue in a process mimicking developmental processes, and that we used to compare to standard myocardial tissue constructs containing only CMs and FBs under both normoxic and injured conditions.

It is known that early during heart development, clusters of proepicardial cells migrate around the heart to form a mesothelial layer known as the epicardium.^[8,9] Once this layer has been established, EPDCs form through EMT and then migrate into the myocardium, contributing to populations of cardiac FBs and vSMCs.^[8,9] Some aspects of this phase of heart development are mimicked by our EPI biowire model in two stages. The first stage involved the formation of an EPI layer around the entire myocardial tissue (days 1–2). Subsequently, in the presence of CMs and cell culture conditions that support the EMT process, we observed a spontaneous migration of EPIs into the cardiac tissue over several days of culture (days 4–8), analogous to the migration of EPDCs into the myocardium during development. Furthermore, these EPIs have morphology consistent with that of cells having undergone EMT. Indeed, while epicardial marker, WT1, was retained in the EPIs as they migrate into the tissue, a decrease in its relative expression was observed when comparing early formed tissues to later stage tissues. While a large proportion of EPIs move into the tissues, some remain on the outer layer of the tissues, likening itself to the native cardiac structure.

Culture of biowire cardiac tissues under normoxic conditions was carried out for over two weeks. Since in our previous studies, cardiac tissues seeded with CMs in monoculture without FBs did not compact,^[29] here, both the control tissues without EPI cells and the EPI cardiac tissues contained FBs such that the comparisons between these groups were not affected by the ability to

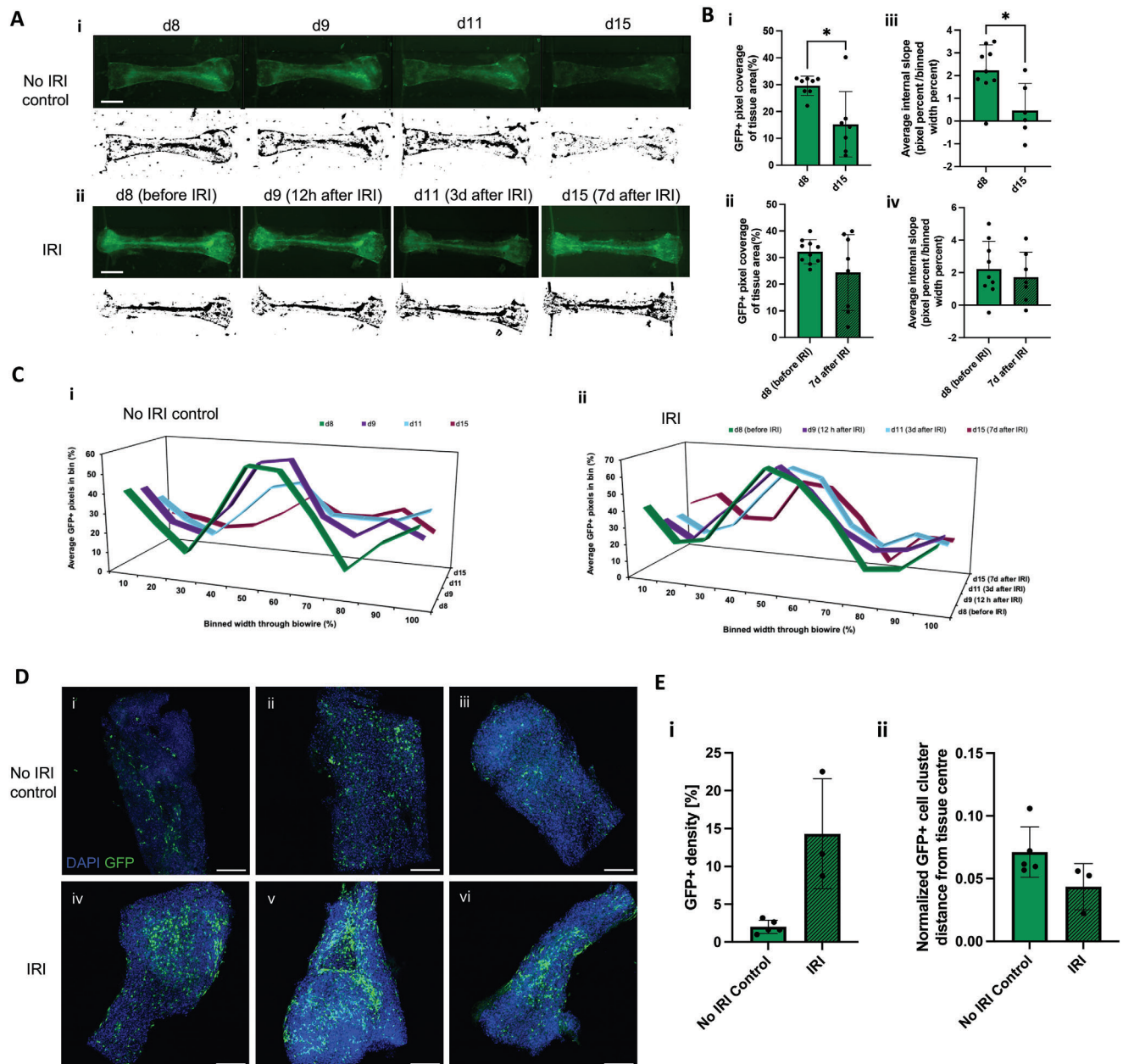


Figure 6. Epicardial cardiac tissues retain stronger EPI cell presence after injury. A) Fluorescence images of GFP+ cells (green) in cardiac tissues (top row) and corresponding thresholded images (bottom row) in CM+FB+EPI cardiac tissues under i) normoxia and ii) with IRI. Scale bar is 500 μm . B) GFP+ area coverage of cardiac tissues compared between day 8 and day 15 (or 7 days after IRI) in i) No IRI control tissues and ii) IRI cardiac tissues. Welch's *t* test was applied. The average internal slope of GFP+ cell distribution profiles in iii) No IRI control tissues and iv) IRI cardiac tissues between day 8 and day 15 (or 7 days after IRI) are also shown. Unpaired *t* test was applied. C) Profiles of the average GFP+ pixels in the binned width through i) No IRI control cardiac tissues and ii) IRI cardiac tissues, comparing day 8 and day 15 (or 7 days after IRI). D) Confocal images of biowire tissues, demonstrating the distribution of GFP+ cells within the tissues (i–vi represent independent tissues). EPI cells are visualized by GFP signal. Nuclei were counterstained with DAPI. Scale bar is 200 μm . E) Quantification of biowire tissues showing i) GFP+ cell density and ii) distance of GFP+ cell clusters from the tissue center relative to the cluster area and tissue perimeter. Welch's *t* tests were performed.

form compacted cardiac tissue structures. Instead, we sought to address the specific contributions of the EPIs and their crosstalk with other cells in 3D cardiac tissue constructs. Initially at day 8, the contractile properties were inferior in the EPI biowire tissues, which may be attributed to the larger cell load. Over time, these properties improved, eventually catching up to the control

tissues whose properties remained stable after formation. However, even at earlier time points, ET and MCR were not different between the control tissues and EPI cardiac tissues, indicating that electrical excitability was similar, which can be explained by the same number of CMs being used in both groups, and indicates that the added EPIs did not impede contraction.

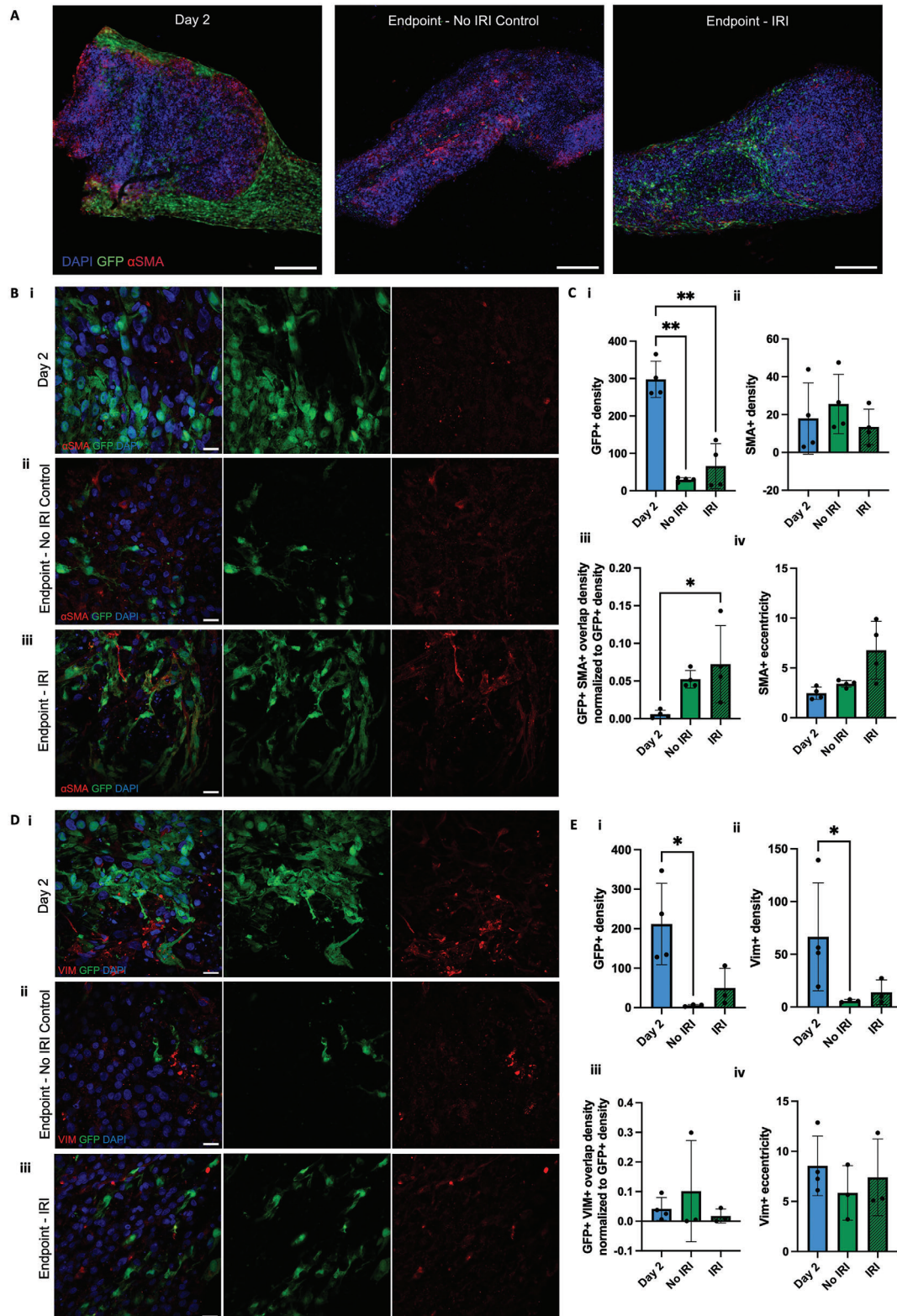


Figure 7. EPI cells display colocalized marker of EMT after injury. A) Confocal images of representative biowire tissues over time, showing presence of GFP+ cells (green) and α -SMA (red). Scale bar is 200 μ m. B) Confocal images of cardiac tissues, showing presence of GFP+ EPI cells (green) and α -SMA+ expression (red) in i) day 2, ii) endpoint No IRI control, and iii) endpoint IRI conditions. Scale bar is 20 μ m. C) Quantification of immunofluorescence images showing ii) GFP+ density (***) and i) α -SMA+ density (*), iii) α -SMA+GFP+ colocalization normalized to GFP+ density (**), and iv) α -SMA+ eccentricity (***) from α -SMA-stained tissues. D) Confocal images of cardiac tissues, showing presence of GFP+ EPI cells (green) and vimentin+

Despite the lower initial contractile properties of EPI cardiac tissues compared to control tissues, the contractile properties of the EPI biowires improved over time through a process that is preceded by a migration of a fraction of the EPIs into the tissues, thus mimicking the contribution of EPIs to the heart through development. Previous studies have shown that engineered heart tissues containing hESC-derived EPIs had the greatest active force compared to groups formed without supporting cells or with supporting MSCs.^[19] Indeed, the hESC-derived EPIs enhanced the contractility, myofibril structure, and calcium handling in the cardiac tissues constructs.^[19] It is known that epicardial-myocardial crosstalk occurs, but this phenomenon is not fully understood. A recent report has shown that iPS-derived premature EPI cells increase contractility and may induce CM proliferation or enhance CM maturity when in co-culture with CMs.^[18] In both reports showing benefits of EPI cells,^[18,19] the improvements in contractility were observed at day 14, which is consistent with our results.

After development, the epicardium becomes dormant in the adult heart and is only reactivated in response to injury. Animal models of ischemic injury include models of MI via permanent ligation of the left anterior descending coronary artery (LAD), models of IRI via temporary occlusion of the left anterior descending coronary artery, or cryoinjury.^[30–32] Differences exist between these injury models in terms of reproducibility, molecular mechanisms involved in the injury, size and extent of the injury, and the inflammatory response.^[30–32] For example, cryoinjury results in a very reproducible injury size, but it has less physiological relevance than permanent or temporary ligation of the LAD. Permanent ligation is less technically challenging and therefore more reproducible than temporary occlusion. The *in vitro* investigation performed in this work made use of an IRI model designed to mimic the temporary occlusion but tailored to heart-on-a-chip tissue constructs, which has been shown to recapitulate certain key molecular and tissue-level processes of the *in vivo* injury.^[26] Specifically, we investigated the effect of ischemic injury on the cardiac tissues after the initial formation process, using the established method.^[26] The described ischemic conditions recapitulate the *in vivo* ischemic setting by mimicking some of the key extracellular ischemic changes (e.g., acidic pH, hyperkalemia, and lactate accumulation), the rapid change between ischemia and reperfusion conditions, and result in effects that align with the reperfusion process *in vivo*, such as increased apoptotic activity and disorganized cardiac ultrastructure.^[26]

IRI was modeled here, which resulted in cell death and trends of decreasing electrical and contractile properties initially after IRI. While our results over the period of over two weeks under healthy/normoxic conditions revealed that the EPI biowires had more significant increases in functional properties compared to control biowires, we see the reverse trend after injury. By tracking functional properties over the week following injury, overall recovery in force properties over time was observed to a lesser ex-

tent in the biowires that include EPIs. Since the initial day 8 values for some functional properties start lower in the EPI group, our comparisons following injury focused on relative differences within one group over time, so as to be able to track changes that result from the injury itself for each tissue. As such, closest attention was paid to the time-dependent differences within each group. A key observation as a result of injury with regards to the functional properties is that there are overall fewer significant increases over time after IRI in the CM+FB+EPI group, representing less recovery in the CM+FB+EPI group. This is corroborated by a significant lowering of MCR right after injury only in the CM+FB group and the reduced LDH release in EPI biowires. It is plausible that the EPI biowires exhibited less significant recovery because they experienced less significant injury, or by more closely mimicking the native physiological response to cardiac injury. Exact mechanisms should be investigated further, but this result reinforces that it is vital to include EPIs in cardiac injury models, as their impacts may affect responses to injury and subsequent recovery.

By specifically evaluating the role of EPIs within structures representing both healthy and injured tissues, we observed differences in their retention within the tissues as well as their transitions to other cell types, again capturing the importance of including EPIs in heart-on-a-chip models of injury. EPI cardiac tissues that underwent IRI demonstrated retention of the GFP+ cells in the tissue, and no decrease in the GFP+ internal profiles over time. Under ischemia, the core of the tissue would experience the most dramatic ischemic effects due to oxygen diffusion limitations,^[33] and thus is it plausible that the EPIs having undergone EMT are more resistant to ischemia and remain at the tissue core as a protective response to maintain tissue viability,^[34] but this would need to be confirmed in future investigations. In this sense, we may be observing a phenomenon that mimics some aspects of the *in vivo* response by the epicardium to injury. Indeed, *in vivo*, ischemia results in death of CMs as well as the activation of EPIs as a compensatory strategy.

α -SMA is expressed by smooth muscle cells and myofibroblasts,^[35] and is considered a marker of the final stages of EMT.^[36] The observation of co-localization of GFP and α -SMA suggests that GFP-expressing EPIs have undergone EMT and transitioned to a smooth muscle or myofibroblast phenotype. It is known that in the infarcted heart, cardiac FBs convert to α -SMA-expressing myofibroblasts, which secrete collagen and matrix proteins.^[37] Myofibroblasts play an important role in both repair post-MI as well as the fibrotic response and contribute to scar formation.^[35] While cells of the epicardial layer undergo change after injury, it has been found that newly activated EPDCs do not populate the infarct region to the same extent as pre-existing epicardium-derived fibroblasts after MI, and that the pre-existing cells contribute more to fibrosis.^[38] In our epicardial biowire model, the epicardial-derived cells invade myocardial tissue at the stage preceding IRI. Therefore,

expression (red) in i) day 2, ii) endpoint No IRI control, and iii) endpoint IRI conditions. Scale bar is 20 μ m. E) Quantification of immunofluorescence images showing i) GFP+ density (*), ii) vimentin+ density (**), iii) vimentin+GFP+ colocalization normalized to GFP+ density (*), and iv) vimentin+ eccentricity (***) from vimentin-stained tissues. Ordinary one-way ANOVA with Tukey's multiple comparisons test (*), Kruskal–Wallis test with Dunn's multiple comparisons test (**), or Brown–Forsythe and Welch ANOVA test with Dunnett's T3 multiple comparisons test (***) were performed. EPI cells are visualized by GFP signal. Nuclei were counterstained with DAPI.

the increased overlap of α -SMA with EPDCs is an indication that this heart-on-a-chip system provides a useful platform to capture responses to injury that correspond to those which occur in vivo, in a way that is novel within engineered heart-on-a-chip systems.

4. Limitations and Future Work

While this study is first to capture certain stages of epicardial contribution to cardiac tissue development and injury in a heart-on-a-chip system, it is important to note that the maturation status of EPIs, which could be revealed through measurements of developmentally staged genes, was not conducted in this work. This would be an interesting future step that could facilitate the inclusion of additional chemical or mechanical features to control the cellular developmental stages within the cardiac tissues over time. A well-known challenge associated with technologies that make use of differentiated stem cell protocols is cellular heterogeneity.^[39,40] As such, it is likely that the hESC-derived epicardial cells in this work differ in maturity and phenotype from epicardial cells of the native cardiac environment post-development due to the inherent immaturity of the cell source. Therefore, it should be understood that the system described in this work is one attempt to model the development and function of cardiac tissue using cell populations that are relatively immature. Future work is therefore needed to more closely recapitulate the mature native cardiac cellular environment, especially for late-onset disease models, by drawing on maturation processes for stem-cell derived cells^[41] or adding in additional maturation processes for the engineered tissues such as long-term electrical stimulation.^[16] Furthermore, while the migration of EPIs occurred in the first week of biowire formation, our investigation of the effects of injury was performed on still relatively immature tissues. Further maturation of the tissues using known electrical field conditioning methods,^[16] was omitted here to enable benchmarking of the baseline effects. It could be undertaken in future studies to generate progressively more mature tissues, such that comparisons of injury response can be performed on “aged” tissues, coupled with deeper investigation of EMT markers.

With more focus applied to the developmental stages of EPIs in the tissue, several additional future directions building off this work could be taken. It may be possible to retain a portion of EPIs at their mature epicardial state around the border of the myocardial tissue using chemical inhibitors of EMT, thus limiting the transition to epicardial-derived fibroblast populations. This way, the cardiac tissue consisting of both EPDCs within the myocardium and an intact mature epicardial cell layer around the edge may be achieved, moving toward a more complete model of the native cardiac environment. Elimination of fibroblast addition to the tissues may also be possible in future studies, relying on EPI as a sole source in a more developmentally faithful paradigm. Finally, we envision our epicardial biowire system being useful for investigations of treatments that could mitigate fibrotic responses and help achieve tissue regeneration after injury. Indeed, the epicardium activated by injury is a source of EPDCs and cytokines that contribute to angiogenesis and revascularization,^[11,42] thus opening up the potential for use of this EPI biowire model for investigations of regenerative strategies.

In terms of the platform, the Biowire II platform has been thoroughly optimized,^[43] with recent enhancements to the platform addressing certain challenges by incorporating features like printed polymer ink and a 24-well plate system.^[44] New challenges based on the work reported here include the two-step seeding protocol used to develop the desired tissue complexity and composition. Future directions to improve tissue generation could include automation of the seeding steps to produce tissues with even greater consistency in terms of distribution of the cell types during tissue formation.

5. Conclusion

This work has established several important steps in the development of more advanced heart-on-a-chip systems. We have shown that we can generate miniature, functional cardiac tissues incorporating a defined layer of epicardium around a myocardium using our Biowire II platform, through a two-step seeding protocol with EPIs added after tissue formation. We were able to mimic the developmental migration of EPIs into the myocardial tissue and demonstrated the ability to track EPI migration and phenotype within the beating cardiac tissues. While EPI biowires had lower contractile forces compared to control biowires initially, they catch up over the following week in culture, demonstrating the ability to form comparably functioning tissues with higher degree of cell complexity. Investigations of these tissues in conditions mimicking IRI revealed that EPI biowires experience less significant cell death during reperfusion, less impact of functional properties such as MCR, and as a result less recovery over time compared to control cardiac tissues. EPI cardiac tissues that underwent IRI had a more pronounced GFP+ signal, indicating a greater EPI cell presence than EPI tissues under healthy/normoxic conditions, with a pronounced migration of cells to the interior. They also exhibited a significant overlap between GFP-expressing EPIs and α -SMA expression. Overall, we observed differences in cardiac tissues with and without EPIs under normal and injured conditions, as well as specific differences in the EPI location and expression as a result of injury, which support that this heart-on-a-chip system containing EPIs provides a useful platform to investigate cardiac processes in development and in response to injury.

6. Experimental Section

Plate Fabrication: Polystyrene plates with repeating rectangular microwells (5 mm × 1 mm × 0.3 mm) and grooves (75 mm × 0.2 mm) were fabricated according to recently established methods.^[45] Briefly, a polystyrene base plate with built-in carbon electrodes was fabricated by using AutoCAD to design a photomask, soft-lithography to create an SU-8 master mold, and polydimethylsiloxane (PDMS, Sylgard 184 silicone elastomer kit, 5:1 ratio of elastomer to crosslinker) poured onto the SU-8 mold to generate a negative mold that was bonded to a silicon wafer via plasma treatment. Carbon electrodes (Cat No. AR-14, Ohio Carbon Blank, 1 mm × 0.4 mm × 96 mm) were incorporated by placing them on the PDMS mold (with distance between two electrodes of 5 mm) and loading into a hot embosser (EVG 520). Thermal bonding at 180 °C and compression force of 3000 N was used to fabricate the base plate.

Microwires were fabricated using nanocomposite ink which was printed directly on the base plate. To fabricate the ink, TPE/QD nanocom-

posites were prepared by mixing core-shell CdSe/ZnS quantum dots and poly(styrene) (ethylene/butylene)-(styrene) copolymers thermoplastic elastomers (TPE) in toluene as previously described.^[45] The final mixture of QDs in the nanocomposite reached a concentration of 0.05 w/w%, after casting them in a glass Petri dish to allow solvent evaporation and baking in an oven under vacuum at 75 °C for 2 h. An array (75 mm × 94.5 mm) of micro-wires (60 μm diameter) was deposited from this nanocomposite ink onto the polystyrene base plate with built-in carbon electrodes by extrusion 3D printing (RegenHU Ltd., Switzerland). The polystyrene plate base fitted with electrodes and microwires was then assembled onto a bottomless 24-well plate using polyurethane glue (two-part adhesive casting system; GS Polymers, cat. No. 1552-2T50).

A microscale mechanical tester (MicroSquisher, CellScale) with customized probes was used to generate the force-displacement curves of the microwires. The probe was placed beside the middle of the nanocomposite wires (60 μm diameter) and moved forward at 2.5 μm s⁻¹ with force applied perpendicular to the long axis of the wire. The force-displacement curves were generated as previously described^[45] and were used to calibrate the contraction force of the biowire tissues.

For one supporting experiment (Figure S9, Supporting Information), polystyrene strips with microwells and poly(octamethylene maleate (anhydride) citrate) microwires were assembled according to previous reports.^[16] Force-displacement curves were also generated as previously described.^[16]

Plates were filled with 70% ethanol for several hours for sterilization and rinsed with phosphate buffered saline (PBS). Prior to cell seeding, 5% w/v Pluronic acid in distilled water was added to the wells for several minutes before removal, and remaining liquid was allowed to evaporate.

Cell Culture: hES2-GFP hPSCs were used for differentiation into pro-epicardial cells adapted from a previously published report.^[27] The eGFP gene is inserted in the ROSA26 locus. Differentiation was performed in embryoid bodies (EB, day 1–4) and monolayer culture (day 4–8) under hypoxic conditions (5% CO₂, 5% O₂, 90% N₂). Briefly, hPSC populations (hES2-GFP) were dissociated into single cells using TypeLE and re-aggregated to form EBs in StemPro-34 media containing 1% penicillin/streptomycin, 2 mM L-glutamine, 150 mg mL⁻¹ transferrin, 50 mg mL⁻¹ ascorbic acid, 50 mg mL⁻¹ monothioglycerol, 10 μM ROCK inhibitor Y-27632 and 1 ng mL⁻¹ rhBMP4 for 24 h on an orbital shaker (70 rpm). On day 1, the EBs were transferred to mesoderm induction media consisting of StemPro-34 with the above supplements (-ROCK inhibitor Y-27632) and 3 ng mL⁻¹ rhBMP4, 1 ng mL⁻¹ rhActivinA and 5 ng mL⁻¹ rhbFGF. On day 4, cells were replated in medium containing 2 μM Retinol, 10 ng mL⁻¹ rhBMP4, 6 μM SB431542, and 1 μM CHIR until day 6. From day 6 to 8/9 cells are cultured in StemPro34 medium. On day 8/9 the population was dissociated into single cells (ColB followed by TrypLE) and cryopreserved for subsequent experiments. eGFP gene expression was found to remain stable throughout differentiation in all lineages analyzed, independent of germ layer.^[46]

The cryopreserved GFP tagged pro-epicardial cells (day 8–9) were used to generate EPIs as follows. The pro-epicardial cells were thawed and plated on 0.1% porcine gelatin-coated six well plates at 200 000 cells per well. Cells were cultured with supplemented Stempro34 media containing 1% penicillin/streptomycin, 1% glutamine, 50 μg mL⁻¹ ascorbic acid, 0.026% (v/v) monothioglycerol, and 6 μM SB (dissolved in DMSO at 18 mM) for 16–20 days, until fully confluent. For dissociation, the monolayers were treated with 1 mg mL⁻¹ collagenase B for 1 h. Detached monolayers were harvested and 0.4% (v/v) TrypLE was added to the cell solution and incubated at 37 °C for 3 min to allow cells to dissociate with gentle pipetting. TrypLE was diluted with media and pelleted at 1200 rpm for 5 min. The pellet was washed with media, recentrifuged, and maintained in minimal media on ice until seeding.

Human ventricular cardiac fibroblasts (FBs) (Lonza CC-2904) were cultured with supplemented Fibroblast growth media 3 (Promocell C-23025) with 1% 10 000 U mL⁻¹ penicillin/streptomycin in a tissue culture flask and passage three to five was used in the biowires. FBs were dissociated with Trypsin for 3 min at 37 °C, neutralized with media and centrifuged at 300 g for 5 min. Cells were resuspended in media, counted, and kept on ice prior to use.

In a supporting experiment (Figure S10, Supporting Information), BJ1D-iPSC derived CMs were used. Briefly, BJ1D iPSC were cultured and passaged into GFR Matrigel (Corning, 354230) coated 12-well plates for CM differentiation according to the protocol described in Lian et al.^[47] On day 20 of differentiation, each well of CMs was incubated in 800 μL of 200 units mL⁻¹ type II collagenase (Worthington, LS004205) and 10 μM ROCK inhibitor (Y-27632 2HCl; Selleckem, S1049) for 1 h. 200 μL of TrypLE-Express (Gibco, 12605010) was then added, and cells were released from the culture surface by gentle pipetting up to 8 times using a P1000 pipette to dissociate clumps. Dissociated cells in solution were diluted 1:1 with blocking media consisting of DMEM containing 10% embryonic stem cell qualified fetal bovine serum (Gibco, cat# 10439024), 1% penicillin/streptomycin, 10 μM ROCK inhibitor, and 10 μM DNase (Calbiochem, 260913-10MU). Prior to use, CMs were counted then centrifuged at 300g for 5 min to remove dissociation media.

In all other experiments, iCell CMs (Cellular Dynamics, 01434) were used. iCell CMs were thawed from frozen according to the manufacturer's instructions, transferred to a falcon tube and diluted with Induction 3 Medium (I3M) (supplemented Stempro34 media containing 1% penicillin/streptomycin, 213 μg mL⁻¹ 2-phosphahte ascorbic acid, 150 μg mL⁻¹ transferrin, 20 mM HEPES and 1% GlutaMAX), followed by centrifugation at 300g for 5 min. Cells were resuspended in media and counted.

Flow Cytometry: A portion of EPI cells that were dissociated for seeding into biowires were set aside for analysis by flow cytometry (Cytek Aurora (violet (405 nm), blue (488 nm), and red laser (640 nm)), Fremont, California, USA). These cells were stained using AldeRed ALDH Detection Assay (Sigma-Aldrich, SCR150) according to the manufacturer's instructions. Cells were also stained for CD105 (Thermo Fisher, 17-1057-42, 1:20) in the AldeRed assay buffer for 30 min at 4 °C. Unstained, isotype control (Thermo Fisher, 17-4714-82, 1:20), and DEAB inhibitor of AldeRed ALDH Detection Assay (Sigma-Aldrich, SCR150) were included. All events were gated by their forward scatter area (FSC-A) versus side scatter area (SSC-A), followed by doublet exclusion based on FSC-A and forward scatter height (FSC-H). This gating was applied to all samples to identify single cells. AldeRed positive events were identified based on SSC-A versus AldeRed fluorescent intensity according to the manufacturer's instructions. CD105 gating was established using the isotype control in the fluorescent intensity histogram. Spectral unmixing was not performed for this experiment since it was a single color assay. All EPI cells were tagged with GFP and equally represented across all samples. The flow cytometry results were analyzed in FlowJo v10.10 Software (BD life sciences).^[48]

Biowire Generation: Biowire tissues were prepared similarly to previous reports.^[16] Cells were suspended in a hydrogel for seeding into the microwells. The hydrogel was prepared by mixing, in order, 10% v/v Medium 199 10x, 10% v/v 2.2 mg mL⁻¹ NaHCO₃, 0.6% v/v 1 M NaOH, distilled water at a volume adjusted to achieve the required final concentration based on the collagen concentration, 3 mg mL⁻¹ collagen I, and 15% v/v GFR Matrigel. The pH was measured to ensure a pH of 7 was achieved, and minute amounts of 1 M NaOH were added to adjust if needed.

For the first cell seeding on day 0, CM and FB cell solutions were combined and mixed, such that concentrations of 90 000 CMs and 10 000 FBs per biowire tissue were achieved. Cells were centrifuged and supernatant was removed from the cell pellet. Hydrogel was added and mixed with the cell pellet in a concentration of 50 000 cells μL⁻¹. The cell-hydrogel suspension was mixed well with gentle pipetting, ensuring minimal bubbles were formed. 2 μL of cell-hydrogel suspension was seeded into each microwell of the plate and left for 10 min at 37 °C to gel. After evidence of gelling was observed, 1.5 mL of I3M was added to each well and plates were incubated at 37 °C.

Seeding of EPIs took place one day after CM/FB seeding. Similar hydrogel was added to the detached and centrifuged EPIs to achieve a concentration of 50 000 cells μL⁻¹ hydrogel. Media was removed carefully from the biowire wells and from the chamber around the slightly compacted biowires, with care taken to not disturb the tissue. 1 μL of EPI-hydrogel suspension was pipetted around the tissue in each microwell, and the plate was transferred to 37 °C for 10 min for gelling to occur. Afterward, 1.5 mL I3M was added to each well. Media was removed and replaced with 1 mL

fresh media on day 5 and day 7. Optical images of biowires were taken over the next week. In some cases, biowires that had adhered to the wall of the chamber were prodded gently with a sterile needle on day 3 to encourage tissues formation. Both CM+FB and CM+FB+EPI tissues were cultured in two separate batches each for the analyses involving functional properties. An additional batch of CM+FB and CM+FB+EPI biowires was cultured for additional immunostaining.

Biowire Functional Properties Assessment: Biowire tissues were assessed for electrical properties through previously described methods.^[16] Briefly, the carbon electrodes in the 24-well plates were connected to a stimulator (Grass Technology S88X Square Pulse Stimulator) and kept at 37 °C in a chamber under the fluorescence microscope for imaging for assessment of functional properties. Tissues were imaged in brightfield, and tissue specific parameters for functional property calculations such as tissue thickness, chamber width, length of tissue attached to wire, and wire passive tension were measured.^[16] The ability of tissues to beat spontaneously (i.e., without additional electrical stimulation) was recorded. ET of each tissue was defined as the minimum voltage required to achieve synchronous beating across the tissue. This was assessed by setting stimulation frequency to 1.00 Hz or 2.00 Hz (depending on spontaneous tissue beating frequency), setting the voltage to 1.00 V cm⁻¹ and increasing the voltage until continuous and synchronized beating for the tissues was observed. The stimulation for testing is monophasic with pulse duration of 2 ms. The frequency used for this measurement was kept constant for each tissue for the assessments over time. The results in the manuscript show the ET value in the units of V. The distance of electrodes is 0.5 cm, and this is consistent for all tissues. With stimulation voltage set to double the ET (to ensure continuous beating), and frequency initially set to 1.00 Hz, MCR of each tissue was measured by gradually increasing the stimulation frequency until beating was no longer controlled by electrical stimulation, specifically noted by a large break in beating. For the supporting experiment with BJ1D-derived CMs, a value of zero was assigned for MCR of tissues that were not beating or not being affected by stimulation, while ET for these tissues was not included.

Videos of the movement of the microwires to which biowire tissues were attached were captured as the tissues beat with increasing stimulation frequency. The wires fluoresce in the Texas Red channel ($\lambda_{\text{ex}} = 596$ nm $\lambda_{\text{em}} = 620$ nm) due to the incorporation of quantum dots, enabling wire movement to be tracked in situ. Videos were taken with spontaneous tissue beating and beating with stimulation at a frequency of 1.00 Hz with voltage set to double the ET. Videos were cropped using Fiji such that a 50-pixel region in the center of the wire was isolated for analysis in a custom MATLAB code. Using this code, wire movement was tracked and translated into functional properties.^[45] Biowires are assumed to be cylindrical in the center region between the wires. In the supporting experiment with BJ1D-derived CMs, for tissues that were no longer beating or not catching, values of zero were assigned for active tension and contraction slope, while values for passive tension were not included as these could not be assumed.

Biowire Injury and Cell Death Assessment: IRI was executed according to an established protocol.^[26] Briefly, to mimic ischemia, regular media was removed from around the biowires, saved at -20 °C, and replaced with ischemic solution (119 mM NaCl, 12 mM KCl, 1.2 mM NaH₂PO₄, 1.3 MgSO₄, 0.5 MgCl, 0.9 CaCl₂, 20 mM sodium lactate, and 5 mM HEPES, pH = 6.4). Minimal solution volume (0.5 mL per well) was used to encourage waste buildup. The plate was transferred to a hypoxic chamber perfused with anoxic gas (95% N₂, 5% CO₂) at 37 °C for 6 h. Ischemic solution was removed, saved at -20 °C, and replaced with reperfusion media (RPMI 1640 supplemented with 1.4 mM calcium chloride and 2% (v/v) B27 without antioxidants (ThermoFisher 10889038) at pH = 7.4), also at 0.5 mL per well. The plate was moved back to oxygenated environment in a 37 °C incubator with a mixture of air and 5% CO₂ for 3 h. After this time, the reperfusion media was removed, saved at -20 °C, and replaced with I3M at a volume of 1 mL per well. Biowires were assessed for spontaneous beating immediately after reperfusion. Functional assessments of tissues were performed according to the previously described procedure^[16] at time points up to 7 days after IRI. An additional 0.5 mL fresh I3M was added four days after IRI.

Lactate dehydrogenase (LDH) assay (Cayman Chemical 601170) was performed on the frozen media from the various stages of the IRI procedure according to manufacturer's instructions. Absorbance values of blank media from the respective media types were subtracted as background.

Tissue assessments were performed 12 h after the end of the IRI procedure, 3 days after the end of the IRI procedure, and 7 days after the end of the IRI procedure. In the baseline tissues (i.e., no IRI controls), assessments were performed and at the same time as the injured tissues, which correspond to day 9, day 11/12, and day 15/16, the last of which is considered endpoint. For simplicity, these timepoints are written throughout as day 9, day 11, day 15.

GFP+ Cell Tracking within Biowires: Tissues were fluorescently imaged (Olympus IX81) to assess location of GFP+ EPIs. Images of biowires taken in the FITC channel were processed and analyzed using Fiji software. Background subtraction with rolling ball radius of 50 was performed, followed by default auto threshold. At three locations across the biowire, a line was drawn, and plot profile was performed to indicate pixel values across the biowire. Pixel values were converted to binary values representing either white or black pixels, which were then binned at 10% intervals of width across the biowire to determine distribution of pixels across the biowire width (Figure S2, Supporting Information).

Immunostaining and Microscopy: Plated monolayers of EPIs from the same batches used for biowires were fixed with 4% paraformaldehyde (PFA) and immunostained for Wilm's Tumor Protein (WT1) and Zonula occludens-1 (ZO1). For WT1 staining, permeabilization with 0.25% Triton X-100 was performed after fixation for WT1 stained cells. Blocking with 10% normal goat serum (NGS) for 1 h at room temperature (RT) was performed prior to incubation with primary antibodies. Anti-WT1 (Abcam, ab 89901 at 1:50 in 10% NGS) and anti-ZO1 (Thermo Fisher 61-7300 at 5 $\mu\text{g mL}^{-1}$ in 10% NGS) were applied overnight at 4 °C. Secondary antibody (Goat-anti-rabbit AF647, Invitrogen A21245, 1:500 in 10% NGS) was incubated for 1 h at RT, followed by DAPI (1:1000). Wells were imaged by fluorescence microscopy (Olympus IX81) and quantified by counting using Fiji software. WT1+ nuclei were automatically counted and cells with ZO1+ borders were manually counted. The averages of each well from two independent differentiations of cells (two wells each) was used.

Tissues at day 2 of formation, and at the endpoint, were removed from the microwires, washed with PBS, and fixed in 4% PFA at 4 °C overnight for 24 h followed by numerous PBS washes. Biowires were stored in PBS until staining. Tissues were cut in half with a razor blade and blocking buffer (10% NGS + 0.1% TritonX-100) was applied for 1 h at RT with rocking. Anti-vimentin (Abcam ab 8978, 5 $\mu\text{g mL}^{-1}$), anti- α -SMA (Abcam ab5694, 1/200), anti-cardiac troponin T (Invitrogen 13-11, 1:100), and anti-WT1 (Abcam ab89901, 1/200) primary antibodies were prepared in blocking buffer, and tissues were incubated with 100 μL antibody solution overnight at 4 °C (separately). Secondary antibodies were prepared in blocking buffer and tissues were incubated at 4 °C overnight. AF 647 goat-anti-mouse IgG1 (Invitrogen A21240, 1:200) was used for vimentin and cTnT-stained samples, and AF 647 goat-anti-rabbit IgG (Invitrogen A21245, 1:200) was used for α -SMA and WT1-stained samples. After each antibody solution was removed, tissues were washed in fresh PBS and kept in PBS at 4 °C overnight to allow adequate washing of excess antibodies. Images were taken with a confocal microscope (Nikon A1R).

α -SMA, vimentin, cTnT and GFP+ cells quantification analysis was performed on unprocessed images using a MATLAB code with the image batch processor app. Briefly, RGB images were transformed into binary images by selecting an appropriate threshold. For α -SMA, vimentin, and cTnT, the density of each channel was measured by calculating the sum of the pixels. To measure the overlap of two channels, the matrices representing each channel were multiplied. GFP+ colocalization in α -SMA+ expression was calculated by overlapping the GFP and α -SMA channels and dividing them by the GFP+ density. The average of at least three images was plotted for each sample. To measure the eccentricity of α -SMA, vimentin, and cTnT, the binary images were processed using the *regionprops* function, yielding an eccentricity value for each cell cluster in the image.^[49] The percentage of clusters with a value of 0.95 to 1 was measured and plotted.

To measure the distance of GFP+ cells from the tissue center using a MATLAB code with the image batch processor app, the binary images were processed using the *regionprops* function. This step produced outputs that included the center of mass and size of each cell cluster. Next, the distance between the center of mass of each cluster and that of the entire tissue was calculated. To incorporate the effect of the cluster size, these distances were adjusted by multiplying by the size of the cluster and dividing by the average size of clusters in the images. Finally, the average adjusted distance was measured and normalized to the tissue size by dividing it by the perimeter of the entire tissue.

WT1 quantification was performed on unprocessed images using Fiji software. Each image corresponding to a channel was converted into binary images by selecting an appropriate threshold, and applying additional clean up steps to distinguish nuclei, which were then counted using the Analyze Particles function. Overlap between channels was established using the imageCalculator function, followed by subsequent Analyze Particles steps.

The displayed low magnification WT1-stained confocal images were processed using Fiji software and included a subtract background step (rolling ball radius of 50) and consistent change to brightness for the red channel. The displayed high magnification α -SMA and vimentin confocal images were processed using a subtract background step (rolling ball radius of 50), and an additional despeckle step for the red channels. The displayed low magnification α -SMA and vimentin confocal images were processed with a subtract background step (rolling ball radius of 50) on every channel.

Statistical Analysis: All statistics were performed using Prism 9 or 10 software. Sample numbers are included in the figure captions for each test or indicated by individual points on the graph and error bars represent standard deviation. For all electrical and functional data of tissues, outliers were identified using ROUT ($Q = 1\%$) method and removed from the data. In cases when a repeated measures test was used for biowires tracked over time, all data from that biowire sample was removed if it was identified as an outlier.

For comparisons of two groups, normality was checked using Shapiro–Wilk test, and nonparametric test was used if normality was not passed. *F* test was used to compare variances, and Welch’s correction was applied if variances were not equal. For comparisons of more than two groups, normality was checked using Shapiro–Wilk test, and a nonparametric test was used if normality was not passed. Brown-Forsythe was used to check variances. For repeated measures comparisons, one-way ANOVA with Dunnett’s multiple comparisons tests was applied and when values were missing, data were analyzed with a mixed-effects model (REML) rather than repeated measures ANOVA, which cannot handle missing values. Statistical significance is indicated by asterisks on the graphs with $p \leq 0.05$ considered significant.

Supporting Information

Supporting Information is available from the Wiley Online Library or from the author.

Acknowledgements

The authors thank the Landon Edgar lab for use of flow cytometry equipment. The authors thank Marie-Jo Abdul-Hay, Felipe Jimenez, Dana Park, and James Ryan Smith for their assistance with data analysis. This work was funded by the Heart and Stroke Foundation Grant-in-Aid G-18-0022356, National Institutes of Health Grant 2R01 HL076485, Natural Sciences and Engineering Research Council of Canada (NSERC) Discovery Grant (RGPIN 326982-10), NSERC Strategic Grant (STPGP 506689-17), Canadian Institutes of Health Research (CIHR) Foundation Grant FDN-167274, Canada Foundation for Innovation/Ontario Research Fund grant 36442 and Stem Cell Network Grant IMP-C4R1-3. M.R. was supported by Canada Research Chairs and Killam Fellowship. D.B. held an NSERC-CREATE TOeP scholarship, S.P.G. held an ORT UHN Post-doctoral Fellowship. Q.W. and Y.Z. held CIHR Postdoctoral Fellowships. K.T.W. held an

Ontario Graduate Scholarship. S.O. held a CIHR Canada Graduate Scholarship. S.L. held an EMBO Postdoctoral Fellowship.

Conflict of Interest

M.R. and Y.Z. are inventors on an issued US patent describing the Biowire platform which is licensed to Valo Health. They receive royalty income from this patent. M.R. Q.W. and Y.Z. are inventors on patent applications covering nanocomposite microwires used here.

Author Contributions

D.B. designed the study, designed and performed experiments, analyzed the results, and wrote and edited the manuscript. S.P.G. designed and performed experiments and edited the manuscript. Q.W. designed and fabricated the culture plates, supported the tissue culture experiments, and edited the manuscript. I.F. differentiated the cells, advised on cell culture and the corresponding results, and edited the manuscript. Y.Z. advised on experimental design, performed experiments related to confocal imaging, advised on experiments and analysis related to tissue functional analysis, and edited the manuscript. K.T.W. advised on experimental design, assisted in tissue culture and injury model experiments, and edited the manuscript. S.O. performed experiments related to confocal imaging and analysis of tissue injury, and edited the manuscript. S.L. performed analysis of immunostaining results and edited the manuscript. N.R. advised on experimental design related to tissue culture, assisted in tissue culture experiments, and edited the manuscript. D.F.B. performed experiments and analysis related to flow cytometry. Y.W. assisted in presentation of results. T.N. advised on design of the injury model experiments. G. V.-N. advised on design of the injury model and edited the manuscript. G.K. advised on cell culture and edited the manuscript. S.E. advised on tissue functional analysis and edited the manuscript. M.R. designed the study, designed the experiments, analyzed results, and wrote and edited the manuscript.

Data Availability Statement

The data that support the findings of this study are available from the corresponding author upon reasonable request.

Keywords

cardiomyocyte, epicardium, epithelium, heart-on-a-chip, ischemia, myocardium

Received: August 11, 2023
Revised: March 22, 2024
Published online: May 9, 2024

- [1] E. A. Woodcock, S. J. Matkovich, *Int. J. Biochem. Cell Biol.* **2005**, *37*, 1746.
- [2] N. R. Tucker, M. Chaffin, S. J. Fleming, A. W. Hall, V. A. Parsons, K. C. Bedi, A.-D. Akkad, C. N. Herndon, A. Arduini, I. Papangeli, C. Roselli, F. Aguet, S. H. Choi, K. G. Ardlie, M. Babadi, K. B. Margulies, C. M. Stegmann, P. T. Ellinor, *Circulation* **2020**, *142*, 466.
- [3] C. M. Kofron, U. Mende, *J. Physiol.* **2017**, *595*, 3891.
- [4] G. S. Ugolini, M. Rasponi, A. Pavesi, R. Santoro, R. Kamm, G. B. Fiore, M. Pesce, M. Soncini, *Biotechnol. Bioeng.* **2016**, *113*, 859.
- [5] N. Takeda, I. Manabe, Y. Uchino, K. Eguchi, S. Matsumoto, S. Nishimura, T. Shindo, M. Sano, K. Otsu, P. Snider, S. J. Conway, R. Nagai, *J. Clin. Invest.* **2010**, *120*, 254.

- [6] A. Colliva, L. Braga, M. Giacca, S. Zacchigna, *J. Physiol.* **2020**, 598, 2923.
- [7] Z. Hu, W. Liu, X. Hua, X. Chen, Y. Chang, Y. Hu, Z. Xu, J. Song, *Arterioscler., Thromb., Vasc. Biol.* **2021**, 41, 1408.
- [8] P. Quijada, M. A. Trembley, E. M. Small, *Circ. Res.* **2020**, 126, 377.
- [9] T. J. Streef, A. M. Smits, *Front. Cardiovasc. Med.* **2021**, 8, 750243.
- [10] A. Weeke-Klump, N. A. M. Bax, A. R. Bellu, E. M. Winter, J. Vrolijk, J. Plantinga, S. Maas, M. Brinker, E. A. F. Mahtab, A. C. Gittenberger-de Groot, M. J. A. van Luyn, M. C. Harmsen, H. Lie-Venema, *J. Mol. Cell. Cardiol.* **2010**, 49, 606.
- [11] B. Zhou, L. B. Honor, H. He, Q. Ma, J.-H. Oh, C. Butterfield, R.-Z. Lin, J. M. Melero-Martin, E. Dolmatova, H. S. Duffy, A. V. Gise, P. Zhou, Y. W. Hu, G. Wang, B. Zhang, L. Wang, J. L. Hall, M. A. Moses, F. X. McGowan, W. T. Pu, *J. Clin. Invest.* **2011**, 121, 1894.
- [12] V. Y. Sidorov, P. C. Samson, T. N. Sidorova, J. M. Davidson, C. C. Lim, J. P. Wikswa, *Acta Biomater.* **2017**, 48, 68.
- [13] O. Schneider, L. Zeifang, S. Fuchs, C. Sailer, P. Loskill, *Tissue Eng., Part A* **2019**, 25, 786.
- [14] I. Goldfracht, Y. Efraim, R. Shinnawi, E. Kovalev, I. Huber, A. Gepstein, G. Arbel, N. Shaheen, M. Tiburcy, W. H. Zimmermann, M. Machluf, L. Gepstein, *Acta Biomater.* **2019**, 92, 145.
- [15] M. A. Tamargo, T. R. Nash, S. Fleischer, Y. Kim, O. F. Vila, K. Yeager, M. Summers, Y. Zhao, R. Lock, M. Chavez, T. Costa, G. Vunjak-Novakovic, *ACS Biomater. Sci. Eng.* **2021**, 7, 5215.
- [16] Y. Zhao, N. Rafatian, N. T. Feric, B. J. Cox, R. Aschar-Sobbi, E. Y. Wang, P. Aggarwal, B. Zhang, G. Conant, K. Ronaldson-Bouchard, A. Pahnke, S. Protze, J. H. Lee, L. Davenport Huyer, D. Jekic, A. Wickeler, H. E. Naguib, G. M. Keller, G. Vunjak-Novakovic, U. Broeckel, P. H. Backx, M. Radisic, *Cell* **2019**, 176, 913.
- [17] Y. R. Lewis-Israeli, A. H. Wasserman, M. A. Gabalski, B. D. Volmert, Y. Ming, K. A. Ball, W. Yang, J. Zou, G. Ni, N. Pajares, X. Chatzistavrou, W. Li, C. Zhou, A. Aguirre, *Nat. Commun.* **2021**, 12, 5142.
- [18] J. J. Tan, J. P. Guyette, K. Miki, L. Xiao, G. Kaur, T. Wu, L. Zhu, K. J. Hansen, K.-H. Ling, D. J. Milan, H. C. Ott, *Nat. Commun.* **2021**, 12, 4997.
- [19] J. Bargehr, L. P. Ong, M. Colzani, H. Davaapil, P. Hofsteen, S. Bhandari, L. Gambardella, N. Le Novère, D. Iyer, F. Sampaziotis, F. Weinberger, A. Bertero, A. Leonard, W. G. Bernard, A. Martinson, N. Figg, M. Regnier, M. R. Bennett, C. E. Murry, S. Sinha, *Nat. Biotechnol.* **2019**, 37, 895.
- [20] L. P. Ong, J. Bargehr, V. R. Knight-Schrijver, J. Lee, M. Colzani, S. Bayraktar, W. G. Bernard, S. Marchiano, A. Bertero, C. E. Murry, L. Gambardella, S. Sinha, *Stem Cell Rep.* **2023**, 18, 936.
- [21] E. Y. Wang, N. Rafatian, Y. Zhao, A. Lee, B. F. L. Lai, R. X. Lu, D. Jekic, L. Davenport Huyer, E. J. Knee-Walden, S. Bhattacharya, P. H. Backx, M. Radisic, *ACS Cent. Sci.* **2019**, 5, 1146.
- [22] E. Y. Wang, U. Kuzmanov, J. B. Smith, W. Dou, N. Rafatian, B. F. L. Lai, R. X. Z. Lu, Q. Wu, J. Yazbeck, X.-O. Zhang, Y. Sun, A. Gramolini, M. Radisic, *J. Mol. Cell. Cardiol.* **2021**, 160, 97.
- [23] O. J. Mechanic, M. Gavin, S. A. Grossman, *Acute Myocardial Infarction*, StatPearls Publishing, Treasure Island (FL) **2023**.
- [24] Z.-Q. Zhao, D. A. Velez, N.-P. Wang, K. O. Hewan-Lowe, M. Nakamura, R. A. Guyton, J. Vinten-Johansen, *Apoptosis* **2001**, 6, 279.
- [25] A. Rodríguez-Sinovas, Y. Abdallah, H. M. Piper, D. Garcia-Dorado, *Heart Failure Rev.* **2007**, 12, 207.
- [26] T. Chen, G. Vunjak-Novakovic, *Tissue Eng., Part A* **2019**, 25, 711.
- [27] A. D. Witty, A. Mihic, R. Y. Tam, S. A. Fisher, A. Mikryukov, M. S. Shoichet, R.-K. Li, S. J. Kattman, G. Keller, *Nat. Biotechnol.* **2014**, 32, 1026.
- [28] I. Fernandes, S. Funakoshi, H. Hamidzada, S. Epelman, G. Keller, *Nat. Commun.* **2023**, 14, 8183.
- [29] Y. Zhao, N. Rafatian, E. Y. Wang, N. T. Feric, B. F. L. Lai, E. J. Knee-Walden, P. H. Backx, M. Radisic, *Matrix Biol.* **2020**, 85, 189.
- [30] C. De Villiers, P. R. Riley, *Dis. Models Mech.* **2020**, 13, 046565.
- [31] L. Bacmeister, M. Schwarzl, S. Warnke, B. Stoffers, S. Blankenberg, D. Westermann, D. Lindner, *Basic Res. Cardiol.* **2019**, 114, 1.
- [32] B. D. Polizzotti, B. Ganapathy, B. J. Haubner, J. M. Penninger, B. Kühn, *Nat. Protoc.* **2016**, 11, 542.
- [33] B. Rodriguez, N. Trayanova, D. Noble, *Ann. N. Y. Acad. Sci.* **2006**, 1080, 395.
- [34] A. Beà, J. G. Valero, A. Irazoki, C. Lana, G. López-Lluch, M. Portero-Otín, P. Pérez-Galán, J. Inserte, M. Ruiz-Meana, A. Zorzano, M. Llovera, D. Sanchis, *FEBS J.* **2022**, 289, 2540.
- [35] S. Cherng, J. Young, H. Ma, *J. Am. Sci.* **2008**, 4, 7.
- [36] D. Bannerman, S. Pascual-Gil, M. Floryan, M. Radisic, *APL Bioeng.* **2021**, 5, 021504.
- [37] H. Venugopal, A. Hanna, C. Humeres, N. G. Frangogiannis, *Cells* **2022**, 11, 1386.
- [38] P. Quijada, A. Misra, L. S. Velasquez, R. M. Burke, J. K. Lighthouse, D. M. Mickelsen, R. A. Dirks, E. M. Small, *J. Mol. Cell. Cardiol.* **2019**, 129, 92.
- [39] C. M. Leung, P. de Haan, K. Ronaldson-Bouchard, G.-e.-a. Kim, J. Ko, H. S. Rho, Z. Chen, P. Habibovic, N. Li Jeon, S. Takayama, M. L. Shuler, G. Vunjak-Novakovic, O. Frey, E. Verpoorte, Y.-i.-C. Toh, *Nat. Rev. Methods Primers* **2022**, 2, 33.
- [40] V. Volpato, C. Webber, *Dis. Models Mech.* **2020**, 13, 042317.
- [41] M. X. Doss, A. Sachinidis, *Cells* **2019**, 8, 403.
- [42] N. Smart, C. A. Risebro, A. A. D. Melville, K. Moses, R. J. Schwartz, K. R. Chien, P. R. Riley, *Nature* **2007**, 445, 177.
- [43] E. Y. Wang, J. Smith, M. Radisic, in *Cardiac Tissue Engineering: Methods and Protocols*, (editors: K. L. Coulombe, L. D. Black III). Springer, New York, NY **2022**, pp. 175–190.
- [44] Q. Wu, P. Zhang, G. O'Leary, Y. Zhao, Y. Xu, N. Rafatian, S. Okhovatian, S. Landau, T. A. Valiante, J. Travas-Sejdic, M. Radisic, *Biofabrication* **2023**, 15, 035023.
- [45] Q. Wu, P. Zhang, G. O'Leary, Y. Zhao, Y. Xu, N. Rafatian, S. Okhovatian, S. Landau, T. A. Valiante, J. Travas-Sejdic, M. Radisic, *Biofabrication* **2023**, 15, 035023.
- [46] L. Yang, M. H. Soonpaa, E. D. Adler, T. K. Roepke, S. J. Kattman, M. Kennedy, E. Henckaerts, K. Bonham, G. W. Abbott, R. M. Linden, L. J. Field, G. M. Keller, *Nature* **2008**, 453, 524.
- [47] X. Lian, J. Zhang, S. M. Azarin, K. Zhu, L. B. Hazeltine, X. Bao, C. Hsiao, T. J. Kamp, S. P. Palecek, *Nat. Protoc.* **2013**, 8, 162.
- [48] FlowJo™ Software (for Mac) [software application] Version 10.10. Ashland, OR, Becton, Dickinson and Company, **2023**.
- [49] S. Landau, S. Ben-Shaul, S. Levenberg, *Adv. Sci.* **2018**, 5, 1800506.